OXFORD GENETICS

GENETICS, 2022, 220(3), iyab234
https://doi.org/10.1093/genetics/iyab234
Advance Access Publication Date: 21 December 2021
Investigation

microRNA-252 and FoxO repress inflammaging by a dual inhibitory mechanism on Dawdle-mediated TGF-β pathway in *Drosophila*

Xiaofen Wu,[1,2,†] Kongyan Niu,[1,2,†] Xiaofan Wang,[1,2,†] Jing Zhao,[1,2] Han Wang ,[1,2] Dean Li,[1,2] Hui Wang,[3] Ting Miao,[4] Yun Yang,[1,2] Huanhuan Ma,[1,2] Yaoyang Zhang,[1] Lei Pan,[5] Rui Liu,[3] Hua Bai,[4] and Nan Liu[1,*]

[1]Interdisciplinary Research Center on Biology and Chemistry, Shanghai Institute of Organic Chemistry, Chinese Academy of Sciences, Pudong, Shanghai 201210, China,
[2]University of Chinese Academy of Sciences, Beijing 100049, China,
[3]Singlera Genomics, Pudong, Shanghai 201203, China,
[4]Department of Genetics, Development, and Cell Biology, Iowa State University, Ames, IA 50011, USA,
[5]Key Laboratory of Molecular Virology and Immunology, The Center for Microbes, Development and Health, Institut Pasteur of Shanghai, Chinese Academy of Sciences, Shanghai 200031, China

*Corresponding author: Interdisciplinary Research Center on Biology and Chemistry, Shanghai Institute of Organic Chemistry, Chinese Academy of Sciences, Pudong, Shanghai 201210, China. Email: liunan@sioc.ac.cn
[†]These authors contributed equally to this work.

Abstract

Inflammaging refers to low-grade, chronically activated innate immunity that has deleterious effects on healthy lifespan. However, little is known about the intrinsic signaling pathway that elicits innate immune genes during aging. Here, using *Drosophila melanogaster*, we profile the microRNA targetomes in young and aged animals, and reveal Dawdle, an activin-like ligand of the TGF-*β* pathway, as a physiological target of microRNA-252. We show that microRNA-252 cooperates with Forkhead box O, a conserved transcriptional factor implicated in aging, to repress Dawdle. Unopposed Dawdle triggers hyperactivation of innate immune genes coupled with a decline in organismal survival. Using adult muscle tissues, single-cell sequencing analysis describes that Dawdle and its downstream innate immune genes are expressed in distinct cell types, suggesting a cell nonautonomous mode of regulation. We further determine the genetic cascade by which Dawdle signaling leads to increased Kenny/IKKγ protein, which in turn activates Relish/NF-κB protein and consequentially innate immune genes. Finally, transgenic increase of microRNA-252 and Forkhead box O pathway factors in wild-type *Drosophila* extends lifespan and mitigates the induction of innate immune genes in aging. Together, we propose that microRNA-252 and Forkhead box O promote healthy longevity by cooperative inhibition on Dawdle-mediated inflammaging.

Keywords: FoxO; microRNA-252; Dawdle/activin-like ligand; Kenny/IKKγ; Relish/NF-κB; antimicrobial peptides; lifespan, inflammaging

Introduction

Low-grade, chronic, and systemic inflammation is a prominent aging hallmark across phyla and constitutes a significant risk factor for pathophysiological decline in older individuals (McGeer et al. 1996; Chen et al. 2005; Vlad et al. 2008; Zhang et al. 2013; Guo et al. 2014; Xu et al. 2015). Given such a causal link, this hallmark has been termed "inflammaging" (Franceschi et al. 2000). Importantly, inflammaging in human, mouse, and *Drosophila* requires the activity of a common set of downstream innate immune factors, including NF-κB (Nuclear Factor enhancing the kappa light chains of activated B cells) and antimicrobial peptides (AMPs) (Adler et al. 2007; Zhang et al. 2013; Chen et al. 2014), highlighting conserved consequence associated with dysregulated expression of these genes. However, the intrinsic mechanism that modulates the age-associated induction of innate immune genes has not been fully understood.

Forkhead box O (FoxO) proteins, a family of conserved transcriptional factors from *Drosophila* to humans, have long been associated with longevity control and tissue homeostasis (Kops et al. 2002; Hwangbo et al. 2004; Demontis and Perrimon 2010). We and other groups have identified the binding targets of FoxO protein from aging *Drosophila* (Alic et al. 2011). Among the FoxO targets, the gene Dawdle (*Daw*), encoding an activin-like ligand of the TGF-β pathway, is directly bound, and transcriptionally repressed by FoxO (Bai et al. 2013). However, whether and how FoxO signaling could modulate inflammaging have not yet been investigated.

To combat pathogen infection, *Drosophila* can mount innate immunity including humoral response by expressing AMPs through IMD and Toll signaling pathways (Lemaitre et al. 1995, 1996; Hedengren et al. 1999; De Gregorio et al. 2002) and cellular response that involves melanization, a proteolytic cascade culminating in the formation of melanin that is deposited on microbial

Received: October 08, 2021. **Accepted:** December 03, 2021

invaders (Nappi and Vass 1993; Bidla et al. 2007). In noninfected *Drosophila*, aging can lead to the spontaneous induction of innate immune genes (Pletcher et al. 2002; Cao et al. 2013) and the steroid-mediated recognition-protein has been suggested to contribute to this age-associated inflammatory phenotype (Zheng et al. 2018), though additional mechanisms might be involved. Since studies of bulk gene expression may mask the heterogeneity of alterations across individual cells, specific cell types in complex tissues that mediate inflammaging remain a question to be addressed.

MicroRNAs (miRNAs) are post-transcriptional repressors, which bind to the 3′UTRs of target mRNAs and subsequently elicit RNA-induced silencing complex that requires the Argonaute (AGO) proteins (Lee et al. 1993; Okamura et al. 2004). *Drosophila* Let-7 and miR-125 have been implicated in the regulation of innate immunity (Garbuzov and Tatar 2010). However, the significance and mechanism by which specific miRNA play during adult lifespan remain poorly addressed. Although the isolation of AGO proteins from cultured cells has been used to analyze bound miRNAs and their target genes (Easow et al. 2007; Chi et al. 2009; Malmevik et al. 2015), targetome-wide characterization of miRNA pathways from aging animals has not been available. Here using *Drosophila*, we investigate the miR-regulated processes by profiling the miRNA targetome from young and aged animals and identify Daw as a physiological target of microRNA-252 (miR-252). We further demonstrate a dual inhibitory regulation on Daw by miR-252 and FoxO, which collectively inhibit the constitutive activation of innate immune genes during aging.

Materials and methods

Fly culture and stocks

Flies were cultured in standard media at 25°C with 60% humidity in a 12-h light and 12-h dark cycle unless otherwise specified. Briefly, standard *Drosophila* food contains sucrose (36 g/l), maltose (38 g/l), yeast (22.5 g/l), agar (5.4 g/l), maizena (60 g/l), soybean flour (8.25 g/l), sodium benzoate (0.9 g/l), methyl-*p*-hydroxybenzoate (0.225 g/l), propionic acid (6.18 ml/l), and ddH_2O to make up 1 l of the food. The wild-type (WT) line used was 5905 (FlyBase ID FBst0005905, w^{1118}). All fly lines used in this study have been backcrossed with 5905 for 5 consecutive generations for a uniform genetic background, though consecutive backcrossing may not be sufficient to eliminate all background variation. Fly stocks used in the present study include: pBID-UAS-HA-Ago1 (this study), pBID-UAS-myc-eGFP-3′UTR (this study), pBID-UAS-myc-eGFP-mirTargets 3′UTR (this study), pBID-UAS-HA-Atg8a (this study), UAS-Babo.Q302D (Brummel et al. 1999), pBID-genomic-N(HA)-FoxO (this study), pBID-genomic-miR-252 (this study), pBID-genomic-N(HA)-Atg8a (this study), pBID-genomic-N(HA)-Key (this study), pBID-genomic-N(HA)-Rel-C(HA) (this study), *Mhc*-GAL4 (Bloomington *Drosophila* Stock Center, #55132).

CRIPSR/Cas9 mutagenesis

CRISPR/Cas9 mutagenesis was performed as described previously (Ren et al. 2013). Two sgRNA plasmids for target gene were injected into fly embryo. Single-fly-PCR assays were used to screen mutants. To do this, single fly was homogenized in 50 μl squashing buffer (10 mM Tris buffer (pH 8.5), 25 mM NaCl, 1 mM EDTA, 200 μg/ml Proteinase K), then incubated at 37°C for 30 min, followed by 95°C, 10 min for inactivation. Screen primers for each target genes were listed in Supplementary Table 4. The virgin females carrying the deletion were backcrossed into WT (5905) male flies for 5 consecutive generations for a uniform genetic background, to mitigate background effects.

Plasmid construction

miRNA reporter

The eGFP fragment was amplified from a common lab-used plasmid with primers: F5-ATGGAACAGAAACTCATCTCTGAAGA GGATCTGGTGAGCAAGGGCGAGGAGCT-3′/R5′-TTACTTGTACAG CTCGTCCATGCCG-3′. The mir-Targets sequence was prepared by 2 steps. (1), 2 DNA oligos were synthesized by Sangon Biotech, as: F5′-CGGCTCGAGCTTCACAGCTGGTAGAGCACGGTAGACAGT TCCTATGCAGAGCACGGTAGACAGTTCCTAAGTGTCCTCGGGAG CCCTTATCAGCCTTCCGTCCACAGGCCCTTATCAGCCTTCCGTCC ATTTGCAACCGCAGGACATCTTTACCCAGCAGTATTACTAGACA TCTTTACCCAGCAGTATTATTGGTCTAGACCG-3′/R5′-CGGTCTAG ACCAATAATACTGCTGGGTAAAGATGTCTAGTAATACTGCTGGG TAAAGATGTCCTGCGGTTGCAAATGGACGGAAGGCTGATAAGGG CCTGTGGACGGAAGGCTGATAAGGGCTCCCGAGGACACTTAGGA ACTGTCTACCGTGCTCTGCATAGGAACTGTCTACCGTGCTCTACC AGCTGTGAAGCTCGAGCCG-3′; (2), the 2 single-stranded oligos were annealed into a duplex (99°C for 5 min and then allowed to cool to room temperature). Each fragment was then ligated into the pBID-UAS vector (Wang et al. 2012).

Fly DNA transgene

RT-PCR amplification was conducted using RNA extract from whole flies, with primers: Ago1: F5′-ATGTACCCATACGATGTTC CAGATTACGCTTATCCAGTTGGACAACAGTC-3′/R5'-TTAGGCAA AGTACATGACCTTCTTG-3′. Genomic transgene covering the *FoxO*, *miR-252*, *Atg8a*, *Key*, and *Rel* genes was prepared by PCR amplification from fly DNA extract. Fusion PCR was used between upstream and gene body sequences, or upstream, gene body, and downstream sequences, with PCR primers:

FoxO (N′-HA tag): upstream: F5′-GAGACGGAGACCGAGACGG C-3′/R5′-TTTTGTGAGCTCAGTCGGGC-3′.

F5′-GCCCGACTGAGCTCACAAAA-3′/R5′-AACATCGTATGGGTA CATGGGGTAGAAAAGTTCGTTG-3′; gene body: F5′-TACCCATACG ATGTTCCAGATTACGCTATGGACGGCTACGCGCAGGA-3′/R5′- CAATTGAGCTCTAAGCGAAGCTG-3′; and downstream:

F5′-CAGCTTCGCTTAGAGCTCAATTG-3′/R5′-ACATCTCTTGCA TTGTGCATGC-3′.

F5′-GCATGCACAATGCAAGAGATGT-3′/R5′-CCCACTGAACTGG CCGGTTT-3′.

miR-252:

F5′-AGAGAGCGAGTGCGATTAAA-3′/R5′-CGTTGCTCCGGTGGT CCGGT-3′.

Atg8a (N′-HA tag): upstream:

F5′-GCCCGAGTAAATGTAGCGCA-3′/R5′-AACATCGTATGGGTA CATGATTGCAATGAAGAGGTAATTG-3′; and gene body:

F5'-TACCCATACGATGTTCCAGATTACGCTAAGTTCCAATACA AGGAGGAGC-3′/R5'-TTTTAGCACATGCTCTCCTTATG-3′.

Key (N′-HA tag): upstream:

F5′-TAGATCCGTATCAGCGCGAT-3′/R5′-AACATCGTATGGGTA CATGTCTCCGTTGTCGCGGT-3′; and gene body:

F5′-TACCCATACGATGTTCCAGATTACGCTTCGGACGAAGAGT CATTCGT-3′/R5′-AATTTGTGATATCCGCAACACG-3′.

Rel (N′-HA tag/C′-HA tag): upstream:

F5′-TTGCTCTGGGGCTTCATCGC-3′/R5′-AACATCGTATGGGTA CATAGTCCGTATCAATCCAATATTTCTG-3′; gene body:

F5′-TACCCATACGATGTTCCAGATTACGCTAACATGAATCAGT ACTACGACCTG-3′/R5′-AGCGTAATCTGGAACATCGTATGGGTAA GTTGGGTTAACCAGTAGGG-3′; and downstream:

F5′-GTTCCAGATTACGCTTGATTATGTATTGAATGTTGATCAA TAA-3′/R5′-GCGCATAAGTACATGTATGAT-3′.

Transgenesis

For φC31-mediated site-specific integration, DNA was clone into the pBID vector (Wang et al. 2012), with the insertion site being chromosome 2L: 5,108,448 or 3L: 11,070,538. Fly microinjection and transgenesis followed standard procedures. Transgenic flies were backcrossed with 5905 (FlyBase ID FBst0005905, w^{1118}) for 5 consecutive generations.

Adult emergence assay

Ten vials of one-to-one cross were set and maintained at standard condition. Four days after egg laying, adult flies were dumped. Total number of adult progenies were counted.

Lifespan assay

Adult virgin female flies were collected at the day of eclosion and maintained at 20 flies per vial at 25°C with 60% humidity and a 12-h light/12-h dark cycle. Flies were transferred to new vials every other day and scored for survival. For each cohort, 20 vials (20 adult flies per vial) were used. The Prism software (Graphpad) was used to draw the survival curve and statistical analysis.

AGO1 Rip-Seq

Adult fly lysates

To induce *Ago1* transgene expression in adults, pBID-UAS-HA-Ago1 transgenic flies were recombined with the *Tubulin-GeneSwitch*-GAL4 line, and adult flies were fed with standard media containing 100 μg/ml Mifepristone (Sigma). After 3- or 30- day induction, 200 mg whole flies were collected into a 15-ml centrifuge tube and immediately frozen in liquid nitrogen. Flies were pulverized to fine powder using a liquid nitrogen cooled mortar and pestle. Resulted fine powder was resuspended in 1 ml Hypotonic Buffer (20 mM HEPES (pH 7.9), 2 mM $MgCl_2$, 10 mM KCl, 1 × protease inhibitor (Sigma), 100 U/ml RNase OUT (Invitrogen), 1 mM DTT (Fisher), 100 U/ml SUPERase In RNase Inhibitor, 400 μM VRC (New England Labs, S1402S) in a 1.5-ml microcentrifuge tube and incubated on ice for 20 min. Nuclei were removed by centrifugation at 10,000 g for 20 min. The supernatant was adjusted to 150 mM KCl, 20% glycerol. A total of 20 μl lysates were taken as input sample.

AGO1 immunoprecipitation

Our immunopurification method was modified from Easow's protocol (Easow et al. 2007). A total of 200 μl monoclonal anti-HA conjugated agarose beads (Sigma) were washed once with 1 ml 0.1M glycine-HCl (pH 2.5, Beyotime) and equilibrated with 1 ml 0.2M Tris–HCl (pH 8). The beads were then blocked in 1 ml wash buffer (20 mM HEPES, pH 7.9, Sigma), 150 mM KCl, 20% glycerol (Invitrogen), 0.1% NP-40, 20 U/ml SUPERase In RNase Inhibitor (Ambion) containing 0.23 mg/ml heparin (Sangon Biotech) for 2 h at 4°C with rotation. The ∼980 μl lysates were incubated with the beads for 1 h at 4°C. The beads were collected and washed with 1 ml Wash Buffer for 3 times each for 2 min. A total of 200 μl washed beads were saved as Rip sample.

RNA extraction and analysis

Input and Rip samples were brought up to a total volume of 500 μl with Wash Buffer. The samples were then digested with 1 g/ml Proteinase K and 0.5% SDS for 30 min at 55°C, and RNA was extracted using acid phenol-CHCl3 (pH 4.5, Ambion). Northern blots for miRNAs were described below. qPCR for reporter gene was described below. For RNA-seq, 200–400 ng of RNA was used to generate sequencing library using NEB DNA library prep kit. The quality of libraries was checked by Bioanalyzer 2100 (Agilent). The quantification was performed by qRT-PCR with a reference to a standard library. The libraries were pooled together in equimolar amounts to a final 2 nM concentration. The normalized libraries were denatured with 0.1 M NaOH (Sigma). Pooled libraries were sequenced on the Illumina Miseq platform with single end 100 bp.

polyA-selected RNA-seq

Muscles were dissected from 40 adult flies of indicated ages and homogenized in a 1.5-ml tube containing 1 ml of TRIzol Reagent (Thermo Fisher Scientific). RNA isolation was followed in accordance with manufacturer's instruction. RNA was resuspended in DEPC-treated Rnase-free water (Thermo Fisher Scientific). TURBO DNA free kit was used to remove residual DNA contamination according to manufacturer's instruction (Thermo Fisher Scientific). A total of 1 μg of total RNA was used for sequencing library preparation. PolyA-tailed RNAs were selected by NEB Next Poly(A) mRNA Magnetic Isolation Module (NEB), followed by the library prep using NEBNext Ultra RNA library Prep Kit for Illumina according to manufacturer's instruction (NEB). The libraries were checked and pooled as described above. Pooled denature libraries were sequenced on the Illumina Miseq, NextSeq 550, or Hiseq 2500 platforms with single end 100 bp.

Single nucleus/cell sequencing

Cell isolation

Eight muscles were dissected using a dissecting scissor in 200 μl Schneider's *Drosophila* Medium (Thermo Fisher) and transferred to a tube containing 200 μl ice-cold Schneider's Drosophila Medium. Muscles were dissociated at 500 rpm for 30 min at 25°C in a Thermo-shaker (Eppendorf) in 50 μl of dispase (3 mg/ml, Sigma), 75 μl collagenase I (100 mg/ml, Invitrogen), and 125 μl trypsin-EDTA (0.05%, Invitrogen). The enzymatic reaction was reinforced by Tissue Grinding Pestle (BBI Life Sciences) every 5 min and ceased by adding 10% fetal bovine serum (Gibco). The mixture was passed through a 40-μm cell strainer (FALCON) and centrifuged at 500 g for 5 min at 4°C. After centrifugation, cells were washed with 1 ml ice-cold DPBS (Gibco) solution for 3 times, resuspended in 500 μl DPBS with 0.04% BSA, passed through a 40-μm strainer (Millex) and counted. Ten microliters of the single-cell suspension was stained with PI (YEASEN) and Hoechst 3342 (Invitrogen), loaded on a hemocytometer (QIUJING), and counted under a Leica microscope (DMI6000B, Leica). A final concentration of 900∼1,500 cells/μl with cell viability above 90% was used for the following single cell RNA-seq experiments. The cell suspension was loaded immediately onto the 10× Genomics Single Cell Instrument to minimize the time between cell preparation and chip loading.

Nuclei isolation

Thirty muscles were dissected within less than 5 min and transferred to a tube which was then put in liquid nitrogen immediately to snap freeze. Tissue samples were homogenized using a glass Dounce tissue grinder (Sigma) 10 times with pestle A followed by a 70-μm cell strainer (FALCON), and 20 times with pestle B followed by a 40-μm cell strainer (FALCON) in 2 ml of ice-cold Nuclei EZ lysis buffer (Sigma) with 0.4 U/μl RNaseOut (Invitrogen). Nuclei were centrifuged at 1,000 g for 5 min at 4°C, washed with 1 ml Nuclei EZ lysis buffer with 0.4 U/μl RNaseOut and incubated on ice for 5 min. After centrifugation, the nuclei

were washed in 1 ml Nuclei Suspension Buffer (NSB) consisting of 1× PBS, 1% BSA (absin), and 0.2 U/μl RNaseOut (Invitrogen) for 3 times. Isolated nuclei were resuspended in 1 ml NSB, filtered through a 40-μm cell strainer and counted 10 μl of the single nucleus suspension in NSB was stained with PI (YEASEN) and Hoechst 3342 (Invitrogen), loaded on a hemocytometer (QIUJING), and counted under a Leica microscope (DMI6000B, Leica). A final concentration of 900∼1,500 nuclei/μl was used for the following single nucleus RNA-seq experiments. The nuclei suspension was loaded immediately onto the 10× Genomics Single Cell Instrument to minimize the time between nuclei preparation and chip loading.

Library preparation

The nuclei/cell suspension was loaded for 10× Genomics run following the Single Cell 3′ Reagent Kits v2 User Guide. The Chromium Single Cell 3′ Library Kit v2 (10× Genomics), Single Cell 3′ Gel Beads Kit v2 (10× Genomics), and Single Cell A Chip Kit v2 (10× Genomics) were used for single cell barcoding, cDNA synthesis and library preparation following manufacturer's instructions.

Sequencing

The quality of libraries was checked by Bioanalyzer 2100 (Agilent). The quantification was performed by qRT-PCR with a reference to a standard library. The libraries were pooled together in equimolar amounts to a final 2 nM concentration. The normalized libraries were denatured with 0.1 M NaOH (Sigma). Pooled libraries were sequenced on the Illumina Miseq/Next-seq platform with a paired-end run sequencing of 26 bp on read 1 and 98 bp on read 2.

Quantitative PCR

RT-qPCR

RNA extractions were done as described above. One microgram of total RNA was used for reverse transcription by polyT primers using SuperScript III First-strand synthesis system for RT-PCR (Thermo Fisher Scientific). Analysis was performed using the QuantStudio 6 Flex real-time PCR system with SYBR selected master mix (Thermo Fisher Scientific). The $2^{-\Delta\Delta CT}$ method was used for quantification upon normalization to the RP49 gene as internal control. Primers for target genes were listed in Supplementary Table 6.

Small RNA-qPCR

Total RNA extractions were down as described above. cDNA of miRNA was synthesized using Taqman MicroRNA Reverse Transcription Kit (Thermo Fisher Scientific) according to the supplier's recommendations. RT- and q-PCR primer sets, dme-*miR-252-5p*, and 2S rRNA were purchased form Thermo Fisher Scientific. Analysis was performed using the QuantStudio 6 Flex real-time PCR system with Taqman Universal PCR Master Mix II (Thermo Fisher Scientific). The $2^{-\Delta\Delta CT}$ method was used for quantification upon normalization to the 2S rRNA gene as internal control.

Small-RNA northern

For small-RNA northern, input RNA (3 μg) and Rip RNA (0.1 μg) was fractionated on a 15% TBE-urea precast PAGE gel (Life Technologies) with 1× TBE buffer, and then transferred onto a Hybond nylon membrane (GE Healthcare) with 0.5× TBE buffer. The RNA blots were prehybridized with Ambion Oligohyb (Life Technologies), and then incubated with radioactive labeled RNA probes for ∼12 h to overnight. RNA probes were used and made by the Ambion Maxiscript-T7 In Vitro Transcription Kit (Life Technologies), supplemented with P^{32}-labeled UTP. Oligo DNA templates were prepared by annealing 2 single-stranded DNA oligos into a duplex (99°C for 5 min and then allowed to cool to room temperature). Oligos used were: *miR-34-5p*: 5′-GATAATACG ACTCACTATAGGGAGA-3′/5′-AAAAAATGGCAGTGTGGTTAGCTG GTTGTGTCTCCCTATAGTGAGTCGTATTATC-3′; *miR-277-3p*: 5′-GATAATACGACTCACTATAGGGAGA-3′/5′-TAAATGCACTATCTG GTACGACATAAATGCACTATCTGGTACGACATCTCCCTATAGTG AGTCGTATTATC-3′; *miR-8-3p*: 5′-GATAATACGACTCACTATAG GGAGA-3′/5′-TAATACTGTCAGGTAAAGATGTCTAATACTGTCAG GTAAAGATGTCTCTCCCTATAGTGAGTCGTATTATC-3′; 2S rRNA: 5′-GATAATACGACTCACTATAGGGAGA-3′/5′-TGCTTGGACTACA TATGGTTGAGGGTTGTATCTCCCTATAGTGAGTCGTATTATC-3′.

Bioinformatic analyses

RIP-seq

Sequencing reads were mapped to the reference genome flybase dm6_r6.05 with STAR2.3.0e (Dobin et al. 2013) by default parameters. The read counts for each gene were calculated by HTSeq-0.5.4e (Anders et al. 2015) htseq-count with parameter "-s no." The count files were used as input to R package DESeq (Anders and Huber 2010) for normalization and the Rip-enriched genes were defined at a log2(Rip/Input) cut-off 1 and adjusted *P*-value cut-off of 0.01. To direct compare Rip enrichment of genes between 3 and 30 days, log2FC were quantile normalized. For genome browser visualization, wig files were generated from bam files by IGVTools with parameter "-z 5 –w 25 –e 250" and displayed by IGV-2.3.6 (Robinson et al. 2011). Cumulative fraction for *daw* wig profile was calculated with R ecdf function and *P*-value was calculated with Kolmogorov–Smirnov test by comparing to uniform distributed CDF. GO term analysis was performed by David (Huang da et al. 2009). For miRNA targetome construction, computational predicted miRNA targets were downloaded from TargetScanFly (Kheradpour et al. 2007) and DIANA-microT (Maragkakis et al. 2011) website and scored by their Rip enrichment. The miRNA–mRNA interaction network was displayed by Cytoscape 3.4.0 (http://cytoscape.org).

PolyA-selected RNA-seq

Sequencing reads were mapped to the reference genome dm6 or flybase dm6_r6.05 with STAR2.3.0e by default parameter. The read counts for each gene were calculated by HTSeq-0.5.4e htseq-count with parameters "-s no." The count files were used as input to R package DESeq for normalization and the differential expression genes were set at a *P*-value cut-off of 0.01 and log2FC of 1. GO term analysis was performed by David.

Single cell/nucleus sequencing analysis

Raw data from 10× Genomics were each processed (alignment, barcode assignment and UMI counting) with Cell Ranger (version 3.0.0) count pipeline. The Cell Ranger reference index was built upon the third 2017 FlyBase release (*Drosophila melanogaster* r6.19). Median saturation was calculated as the median of the Sequencing Saturation metric reported by the Cell Ranger software.

Single-nuclei data preprocessing

Reads were filtered to build high-quality single-cell data. A dataset of 10,209 nuclei from WT (FlyBase ID FBst0005905, w^{1118}) and *mir-252*^{c328} *foxo*^{c431} double mutants was generated using a customized method to select the quality nuclei with filtering metrics

applied as follows. First, to remove empty droplets, we used the *emptyDrops* function in DropletUtils (v1.6.1) R package (Lun et al. 2019) with the default parameter. Subsequently, the *isOutlier* function in scater (v1.14.4) R package (McCarthy et al. 2017) was used to detect the outliner nuclei and genes. QC metrics included Unique Molecular Identifiers (UMI), gene expression, the proportion of mitochondrial transcripts, ribosomal protein transcripts, and ribosomal RNA; any one of the criteria failed to pass the quality settings was considered to be of low quality and discarded. Third, we used DoubletFinder (v2.0.2) R package (Kiselev et al. 2019) and *doubletCells* function in scran (v1.14.5) R package (McCarthy et al. 2017) to detect and discard doublet. Finally, we removed the mitochondrial genes, ribosomal protein genes, and ribosomal RNA from sequence reads.

Dimensionality reduction and clustering

The filtered matrix was then used as input for Seurat (Stuart et al. 2019). The Seurat pipeline was executed on a combined dataset of WT and *mir-252*^{c328} *foxo*^{c431} double mutants. Data were log-normalized with a scale factor of 10^4. Variation driven by individual batches was regressed out from the normalized, scaled data. For further downstream analysis, the most variable genes (2,000) were selected using *FindVariableGenes* with default parameters. The graph-based method from Seurat was used to cluster nuclei. The PCA was selected as dimensional reduction technique. To visualize the data, UMAP dimensionality reduction was performed, using the first 50 PCAs, as instructed by a Jack Straw resampling test. Clusters were identified by a shared nearest neighbor, using a resolution of 0.4. And the clusters were confirmed by centroid-based clustering (K-means) and Density-based clustering (HDBSCAN). Some of these clusters were manually modified. A total of 17 clusters were confirmed for the final UMAP.

Markers identification

We used marker genes to infer the predominant cell type within each cluster in Seurat. For clusters, a set of markers genes (Supplementary Table 1) was defined by *FindConservedMarkers* of the nuclei grouped in each cluster against the remaining nuclei. Signature marker genes were defined based on the Wilcoxon rank-sum test with Bonferroni corrected *P*-value ≤ 0.05 and log2 (mean gene expression across nuclei in cluster/mean gene expression across nuclei in other clusters) of 0.25.

Comparison of bulk tissue mRNA with single nuclear RNA transcriptomic profiles

To compare gene expression data between bulk mRNA-seq and sNuc-seq, we performed Pearson's correlation analysis. Only genes that detected in both datasets were used for the analysis. For sNuc-seq data, we calculated the average normalized UMI expression for each gene. For bulk data, gene counts were converted to counts per million reads mapped (CPM). And then log-transformed data was used for the plot. $P < 0.05$ was considered statistically significant.

Differential proportion analysis

To detect changes in cell proportions between WT and mutants, we used differential proportion analysis as described by Farbehi et al. (2019). $P < 0.01$ was considered statistically significant.

Western blot assay

Twenty muscles were harvested and homogenized in a 1.5-ml tube containing 200 µl 2× Laemmli Sample Buffer (BIO-RAD) provided with 5% βME. Samples were then heated at 95°C for 5 min and centrifuged at 10,000 g for 3 min. Resulted supernatant was loaded onto a NuPAGE 12% Bis-Tris Gel (Thermo Fisher Scientific, Carlsbad, CA, USA), and then transferred by electrophoresis to a polyvinylidene fluoride membrane (Millipore, Germany). The corresponding primary antibodies were diluted 1:5,000 and incubated with the membranes at 4°C overnight, the secondary antibodies were diluted 1:5,000 and incubated for 2 h at room temperature. The signals were detected using ECL (Thermo Fisher Scientific) by Amersham Imager 600 (GE Healthcare, Sweden). The signal intensity was quantified by ImageQuant TL (GE Healthcare). Three biological replicates were done for each experiment.

Luciferase assay

Luciferase assay was performed using standard approaches (Liu et al. 2012). Specifically, 1×10^5 S^2R+ cells were plated and bathed in 200 µl complete medium in each well of a 96-well plate. The next day, 8 ng of pIZ-Firefly, 400 ng of pIZ-*miR-252*, and 400 ng of pIZ-renilla-3'UTR (*daw* WT or mutant reporters) were transfected by Effectene (Qiagen). Two days post transfection, luminescence assays were performed by Dual-Glo Luciferase Assay System (Promega). The miR-252 seed sequences in the 3'UTR of Daw gene was noted in Fig. 1c.

Small-RNA sequencing

We followed Wang's protocol in performing small-RNA sequencing (Wang et al. 2016). Fly head and muscle tissues were dissected in ice-cold 1× phosphate-buffered saline solution (Sangon Biotech), and total RNA was isolated using Trizol according to the manufacturer's instructions (Life Technologies). DNA was removed using the Ambion TURBO DNA-free Kit (Life Technologies). RNA was then fractionated using 15% TBE-urea precast PAGE gels (Life Technologies). Small RNA of 20–29 nt was sliced from the gel and recovered using the ZR Small-RNA PAGE Recovery Kit (Zymo Research). To determine library quality, qRT-PCR was used to quantify the library concentration. The normalized libraries were denatured with 0.1 M NaOH solution (Sigma). Pooled libraries with different barcodes were sequenced on the Illumina Miseq platform.

Small-RNA Sequencing analysis

Adapter sequence was removed using FASTX (http://hannonlab.cshl.edu/fastx_toolkit/). Reads without adapter, shorter than 18 nt or mapped to rRNAs were filtered out. For annotating miRNAs, we used miRDeep2 (Friedländer et al. 2008). Drosophila genome release 6 from FlyBase was used as reference. The miRNA precursor and mature miRNAs were from miRBase. miRNA isoform statistics were carried out according to miRDeep2 output, and reads were restricted with perfect match.

Results

miRNA targetomes from young and aged *Drosophila*

To study miRNA pathways, we developed a strategy to generate the miRNA targetome in adult animals by immunoprecipitating AGO1 protein, followed by polyA-selected RNA sequencing (AGO1 RIP-seq) (Supplementary Fig. 1a). We validated this strategy first by confirming the ability of AGO1 pulldown to enrich the mature forms of miR-34-5p (multiple isoforms), miR-277-3p (2 isoforms), and miR-8-3p (single isoform), but not fly 2S ribosomal RNA (Supplementary Fig. 1b). This strategy was further validated

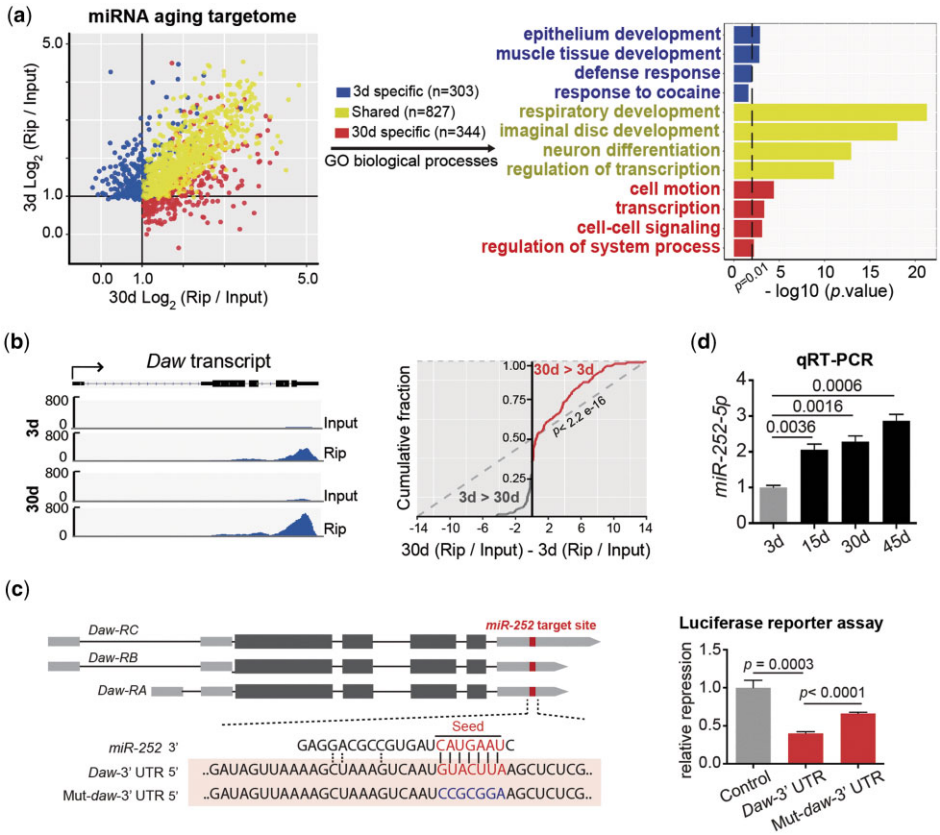

Fig. 1. miRNA targetomes for adult, aging *Drosophila*. a) Scatter plot (left panel) showed AGO1-enriched genes from young and aged flies. Candidate target genes were sorted into 3 categories based on their enrichment at 3 days only (blue), 30 days only (red) or both 3 and 30 days (yellow). Gene Ontology analysis (right panel) indicated enriched biological processes for each category. Dotted line indicates $P = 0.01$. Candidate targets were identified from 2 biological replicates of 3- and 30-day flies (enrichment criteria: log2(Rip/Input) > 1, adj. $P < 0.01$). Genotype: *gene-switch tubulin*-GAL4, pBID-UAST-HA-Ago1 (see *Materials and Methods* for further details). Whole flies were used. b) Genome browser view (top panel) illustrates the Daw transcript in input vs AGO1 RIP-seq profiles. This enrichment was further enhanced with age (bottom panel). The increase of Daw enrichment was calculated by deducting 3-day enrichment from that of 30 days, and was then plotted cumulatively for each 25 bp along the Daw transcript. *P* value was calculated using Kolmogorov–Smirnov test against uniform distribution. c) Potential miR-252 target site in 3′UTR of Daw transcripts (top panel). The site was predicted by both microT_CDS and TargetScan. Blue color illustrated nucleotides mutated to disrupt pairing between miR-252 and Daw. The 3′UTRs of WT or mutant were subsequently cloned downstream of the firefly luciferase. Luciferase assays (bottom panel) revealed a silencing effect between miR-252 and Daw, which was dependent on the WT, but not mutated, miR-252 binding site in the 3′UTR of Daw (for quantification: mean ± SEM of 3 biological repeats; Student's *t*-test). d) qRT-PCR analysis confirmed that miR-252-5p, the guiding strand of miR-252, had an age-dependent increase. qRT-PCR was from muscles of female flies aged at 3, 15, 30, and 45 days. Genotype: 5905 (for quantification: mean ± SEM of 3 biological repeats; Student's *t*-test).

using a miRNA reporter approach. We constructed transgenic flies, expressing a transgene with the coding region for green fluorescence protein (eGFP) fused with either a standard 3′UTR as the control reporter or a miRNA reporter with the 3′UTR embedded with target-mimicking sequences for 3 highly abundant miRNAs in adult flies, miR-276a-3p, miR-184-3p, and miR-8-3p (Supplementary Fig. 1c). In flies that expressed the control reporter and miRNA reporter at comparable levels, AGO1 pull down resulted in 8-fold enrichment of the miRNA reporter compared to that of control (Supplementary Fig. 1c), indicating that this strategy could specifically identify mRNA transcripts actively targeted by endogenous miRNAs. Using this strategy, we systemically analyzed the mRNAs associated with the AGO1 protein by RNA-seq. Inspection of select genes known to be miRNA targets found enrichment by Ago1 RIP-seq (Supplementary Fig. 1d). In contrast, Gapdh2 and AlphaTub84B, 2 housekeeping genes that are not targeted by miRNA, showed no such enrichment (Supplementary Fig. 1d). Combined, these data establish that the AGO1 RIP-seq strategy can be used to profile in vivo miRNA targetome.

We then characterized miRNA targetome in adult flies at 3 d of age (young) and 30 d of age (aged) (Fig. 1a). We set 2-fold enrichment of read counts between IP and input as the cut-off (Supplementary Fig. 1a). Based on 2 independent experiments, we were able to identify 1,130 and 1,171 candidate target genes from young and aged animals, respectively (Fig. 1a and Supplementary Table 1). Among them, 303 candidate target genes were only identified when animals were young (Fig. 1a). Gene Ontology (GO) analysis indicated that their roles were mainly involved in development (Fig. 1a). On the other hand, 344 candidate target genes were unique in aged animals, with known functions involved in post-developmental events, such as cell adhesion, cell fate determination, cell motion, and transcription (Fig. 1a). Of note, 827 candidate target genes were found in both 3 and 30 days, with their biological functions associated with developmental processes (Fig. 1a). It was noteworthy that AGO1-associated mRNA genes tended to express longer transcripts compared to that of nonenriched genes (Supplementary Fig. 2).

Since miRNA profile can directly influence the composition of miRNA targetome, we next determined the expression of miRNAs

during adult lifespan. Small-RNA-seq analysis using head and muscle tissues identified 110 miRNAs expressed in 3- and/or 30-day-old flies (Supplementary Table 2). We subsequently combined miRNA targetome with computational algorithms, microT_CDS (Maragkakis et al. 2011) and TargetScan (Kheradpour et al. 2007), aligning specific miRNAs with their putative targets based on the predicted miRNA binding sites (Supplementary Table 3). Taken together, our findings reveal a network of mRNA targets that might define insights into the miRNA-regulated events in young and aged adult flies.

Daw is a target of miR-252

Targetome analysis identified Daw, a pro-aging factor, that was revealed by our early study (Bai et al. 2013). Daw was significantly enriched in both 3- and 30-day AGO1 RIP-seq profiles; moreover, this enrichment was higher in 30 days than in 3 days (Fig. 1b), implicating an age-modulated, post-transcriptional regulation on Daw by miRNA pathways. Both microT_CDS and TargetScan analyses noted 1 target site of miR-252-5p (hereinafter referred to as miR-252) within the 3′UTR of Daw (Fig. 1c). To determine whether miR-252 could regulate Daw through this site, we generated a Renilla luciferase reporter with the coding region of luciferase fused with the 3′UTR of Daw. This luciferase reporter was transfected into *Drosophila* S2R^{+} cells in the presence of miR-252 overexpression. We found that upregulation of miR-252 led to 60% reduction in the expression of this Daw-3′UTR reporter compared to that of the control reporter (Fig. 1c). We generated a construct with a mutation that disrupted seed pairing between miR-252 and its putative binding site (Fig. 1c). The ability of miR-252 to regulate the expression of this mutant Daw 3′UTR reporter was significantly reduced compared to that of WT reporter (Fig. 1c). These results validated that the silencing effect of miR-252 was dependent on the its binding site in the 3′UTR of Daw mRNA.

miR-252 and FoxO control organismal survival by repressing Daw

Our previous study implicates that Daw gene is transcriptionally repressed by FoxO protein in fly muscle tissues (Bai et al. 2013). Our current data suggested an additional layer of repression on Daw mRNA by miR-252 at the post-transcriptional level. Consistently, small-RNA qRT-PCR analysis from muscle tissues of WT flies revealed that miR-252 had an increase with age (Fig. 1d), correlating with age-augmented enrichment of Daw in the AGO1 RIP-seq (Fig. 1b).

To investigate the biological significance of this dual-inhibitory regulation, we compared adult phenotypes using flies depleted of both FoxO and miR-252 with that of single mutation alone. We used CRISPR/Cas9-mediated genomic editing (Ren et al. 2013) to obtain loss-of-function alleles, *mir-252*^{c328} and *foxo*^{c431} (Supplementary Table 4). Flies lacking FoxO activity had a defect in preadult survival, evidenced by the reduction in the numbers of flies eclosed into the adult stage compared to WT (Fig. 2a). In congruence with a previous study by Yamamoto and Tatar (2011), *foxo* mutant flies, when developed into adult, exhibited a shortened lifespan (Fig. 2b). While *mir-252* mutants alone had little effect on adult emergence (Fig. 2a) or age-associated mortality (Fig. 2b), loss of both miR-252, and FoxO resulted in further decline in pre-adult survival (Fig. 2a) and adult lifespan (Fig. 2b).

To ensure that the mutant phenotypes were attributable to specific genes, we generated genomic transgenes for miR-252 and FoxO, which expressed these genes under their respective endogenous regulatory elements (Supplementary Fig. 3). Restoring the expression of either miR-252 or FoxO to the double mutants rescued adult emergence (Fig. 2c) and adult survival (Fig. 2d), suggesting that these defects were due to the loss of miR-252 and FoxO.

To address whether above defects were caused by an abnormal increase of Daw, we lowered the level of Daw by combining double mutants with *daw*^{c458}, a deficiency mutant generated by CRISPR/Cas9 (Supplementary Table 4). Assessment of adult emergence and adult survival phenotypes revealed rescue effects (Fig. 2, e and f). Altogether, these data indicate that FoxO and miR-252 cooperate in repressing Daw at the transcriptional and post-transcriptional level, respectively (Fig. 2g). Double mutant flies exhibit enhanced defect in organismal survival compared to either single mutant alone, suggesting that FoxO and miR-252 exert a dual-inhibitory effect on *Daw* expression.

Deregulated Daw triggers hyper activation of innate immune genes

Interestingly, we observed that mutant flies carried melanotic tumors, characterized by small black spots deposited in the cuticle of abdomen (Fig. 3a), which is one of the key markers of immune activation in *Drosophila*. Quantitative assessment showed that melanotic tumors were detectable in *mir-252* single mutant (3%) and *foxo* single mutant (8%) at low levels. The extent of melanization was enhanced in *mir-252*^{c328} *foxo*^{c431} double mutants (30%), which was rescued by *daw* deficiency (14%).

Above observation prompted us to investigate global changes of gene expression, especially the innate immune pathways. Since we and other groups have indicated that age-related activities of Daw are associated with muscle tissues in *Drosophila* (Bai et al. 2013; Demontis et al. 2014), we performed polyA-selected RNA-sequencing using primarily thoracic muscles for this and subsequent experiments. GO analysis revealed that “innate immune response” and closely related processes were highly upregulated in *mir-252*^{c328} *foxo*^{c431} mutants, whereas mitochondrial and energy metabolism-related pathways were enriched for downregulated genes (Fig. 3b). This result was validated by qRT-PCR analysis on select genes of innate immune pathways (Supplementary Fig. 4). Furthermore, detailed examination revealed dynamic shift in gene expression of innate immune pathways in different mutant backgrounds. The extent of immune activation was mild in *mir-252* single mutant but became elevated in *foxo* single mutant (Fig. 3, c and d). Such immune activation was further enhanced in *mir-252*^{c328} *foxo*^{c431} double mutants, which can be rescued by *daw* mutation (Fig. 3, c–e). Distinct shifts in gene profiles (Fig. 3c) were correlated with the extent by which Daw was abnormally increased, as well as pathophysiological deteriorations, including melanization, preadult lethality, and reduced lifespan, suggesting that Daw might define an effect that couples innate immune hyper activation with a rapid decline in organismal survival.

It was possible that age-related activity of miR-252 might be mediated by many mRNA targets, in addition to Daw. To address this, we deleted the miR-252 binding site on Daw 3′UTR via CRISPR/Cas9 (Fig. 3f and Supplementary Table 4). We then asked whether this mutant, *daw-3′UTR*^{c82}, recapitulated defects as those conferred by the loss of miR-252 (Fig. 3f). Consistently, *daw-3′UTR*^{c82} *foxo*^{c431}double mutants exhibited preadult lethality (Fig. 3g), melanization (Fig. 3h), and hyper activation of innate immune genes as assessed by the RNA-seq experiment (Fig. 3i), suggesting that age-related activity of miR-252 is mediated mainly

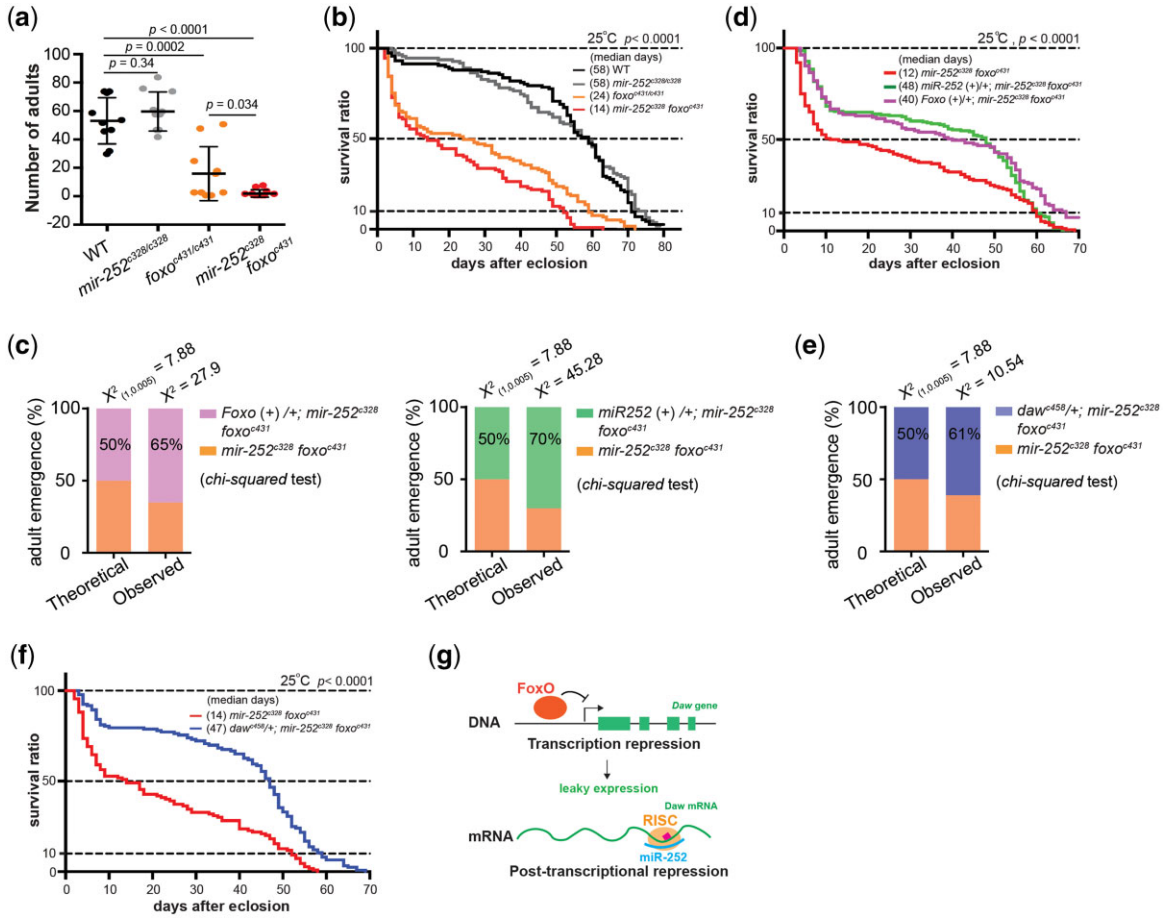

Fig. 2. FoxO and miR-252 promote organismal survival by repressing Daw. a) Flies deficient in both FoxO and miR-252 show strong defect in adult emergence. Eclosed adult flies for indicated genotypes were counted. To name new mutants, a superscript amended to the gene contained a letter c denoting CRISPR/Cas9 method followed by the size of genomic deletion. All mutants have been backcrossed with WT for 5 times to ensure a uniform genetic background (see Supplementary Table 4 and *Materials and Methods* for further details). Genotypes: WT: 5905. *mir-252*$^{c328/c328}$. *foxo*$^{c431/c431}$. *mir-252*^{c328} *foxo*^{c431}: *mir-252*^{c328}, *foxo*^{c431}/*mir-252*^{c328}, *foxo*^{c431} (for fly quantification: mean ± SD of 10 biological repeats; Student's *t*-test). b) Flies deficient in both FoxO and miR-252 show strong defect in adult survival. *foxo* mutants had a shortened lifespan. While *mir-252* mutants alone had little effect on adult survival, flies lacking both FoxO and miR-252 showed a decline in lifespan. Genotypes as in (a) (for lifespan assay: 25°C; $n \geq 200$ female flies per genotype for curve; log-rank test). c) Genomic transgene of FoxO or miR-252 significantly rescues preadult lethality. Based on the mating scheme (top panel), progeny counts of expected and observed genotype were shown (bottom). Genotypes: *mir-252*^{c328} *foxo*^{c431}: *mir-252*^{c328}, *foxo*^{c431}/*mir-252*^{c328}, *foxo*^{c431}. *Foxo* (+)/+; *mir-252*^{c328} *foxo*^{c431}: pBID-genomic-N(HA)-Foxo/+; *mir-252*^{c328}, *foxo*^{c431}/*mir-252*^{c328}, *foxo*^{c431}. *miR-252* (+)/+; *mir-252*^{c328} *foxo*^{c431}: pBID-genomic-miR-252/+; *mir-252*^{c328}, *foxo*^{c431}/*mir-252*^{c328}, *foxo*^{c431}. Chi-square test. d) Genomic transgene of FoxO or miR-252 significantly rescues age-associated mortality. Adding back either FoxO or miR-252 to double mutants significantly rescued adult lifespan. Genotypes as in (c). Lifespan assay as in (b). e) Decreasing Daw significantly rescues preadult lethality. Adult emergence test as in (c), with different mating scheme (top panel) and progeny counts (bottom). Genotypes: *mir-252*^{c328} *foxo*^{c431}: *mir-252*^{c328}, *foxo*^{c431}/*mir-252*^{c328}, *foxo*^{c431}. *daw*^{c458}/+; *mir-252*^{c328} *foxo*^{c431}: *daw*^{c458}/+; *mir-252*^{c328}, *foxo*^{c431}/*mir-252*^{c328}, *foxo*^{c431}. Lifespan assay as in (b). f) Decreasing Daw significantly rescues age-associated mortality. Genotypes as in (e). Lifespan assay as in (b). g) Dual-inhibitory regulation on Daw by FoxO and miR-252, at the transcriptional and post-transcriptional level, respectively.

through Daw and that proper regulation on Daw requires the miR-252 binding site on Daw 3′UTR.

mir-252 and *foxo* mutants advance key features of inflammaging

We next asked how gene profiles in single and double mutants were compared with age-associated activation of innate immune genes that naturally occur in WT aging flies. Consistent with above experiments, we used dissected muscle tissues. We transcriptionally profiled WT animals of 3, 15, 30, and 45 days of age. Comparative analysis of RNA-seq profiles demonstrated that single and double mutants at 3 days already triggered a gene profile of innate immune hyper activation reminiscent of chronic inflammation observed in older WT animals (Fig. 4), indicating that normal activities of miR-252 and FoxO might be critical in prevention of age-associated induction of innate immune genes. Thus, loss of miR-252 and FoxO lead to key characteristics of accelerated inflammaging, evidenced by temporally advanced induction of innate immune genes and consequentially shortened lifespan.

Single-cell sequencing reveals Daw and innate immune genes in discrete cell types

Since our above data showed the induction of innate immune genes at the bulk level, we performed single-cell sequencing to determine the composition and functional states of different cell types in *mir-252*^{c328} *foxo*^{c431} double mutants. Consistent with bulk RNA-seq experiment, we used 3-day-old flies for single-cell analysis. While analyzing single whole-cell suspensions from fly thoracic muscle tissues, we noticed over-represented sequence reads (>90%) from muscle mitochondria (Supplementary Fig. 5a). To avoid this bias, we developed a strategy to isolate individual

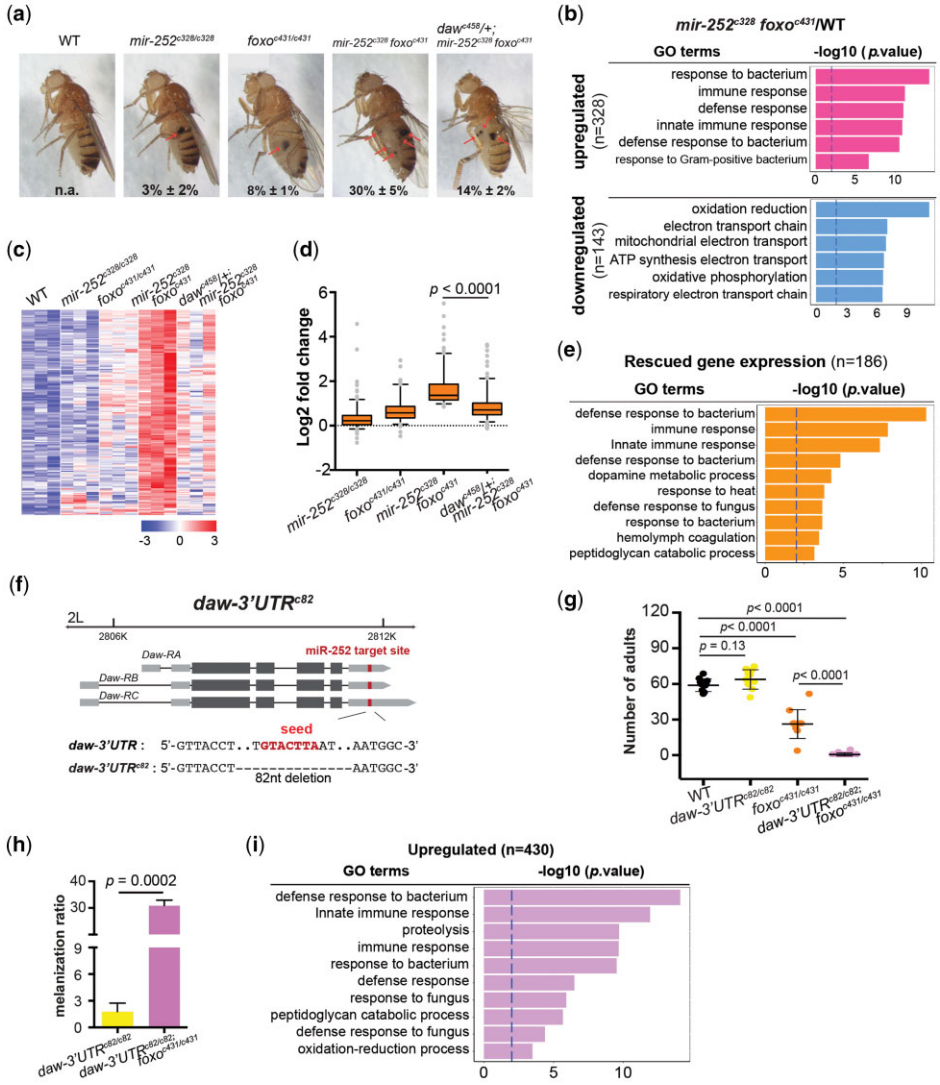

Fig. 3. Deregulated Daw triggers hyper activation of innate immune genes. a) Mutant flies develop melanization marks. Melanotic tumors were highlighted by arrows. For indicated genotypes, the percentage of flies at 3 days of age carrying melanotic tumors was counted. Genotypes: WT: 5905. *mir-252*$^{c328/c328}$. *foxo*$^{c431/c431}$. *mir-252*^{c328} *foxo*^{c431}: *mir-252*^{c328}, *foxo*^{c431}/*mir-252*^{c328}, *foxo*^{c431}. *daw*^{c458}/+; *mir-252*^{c328} *foxo*^{c431}: *daw*^{c458}/+; *mir-252*^{c328}, *foxo*^{c431}/*mir-252*^{c328}, *foxo*^{c431} (for quantification of melanization marks: mean ± SD of 3 biological repeats with more than 50 flies for each replicate). b) GO analysis (biological processes) reveals immune hyperactivation in *miR-252 foxo* double mutants. RNA-seq was from muscle tissues of 3-day-old female flies. Genotypes: WT: 5905. *mir-252*^{c328} *foxo*^{c431}: *mir-252*^{c328}, *foxo*^{c431}/*mir-252*^{c328}, *foxo*^{c431} ($n = 328$ for upregulated genes, log2 (fold change) > 1, adj. $P < 0.01$; $n = 143$ for downregulated genes, log2 (fold change) < −1, adj. $P < 0.01$). c, d) Genes ($n = 186$) upregulated in *foxo miR-252* double mutants but rescued by *daw* deficiency were profiled for Heatmap c) and Box Plot d). Genotypes as in (a). RNA-seq as in (b) (for Box Plot: normalized read counts relative to WT (log2 transformed). Student *t*-test, mean ± SEM. *miR-252*$^{c328/c328}$: 0.34 ± 0.04. *foxo*$^{c431/c431}$: 0.68 ± 0.04. *foxo*^{c431} *miR-252*^{c328}: 1.64 ± 0.06. *daw*$^{c458/+}$; *foxo*^{c431} *miR-252*^{c328}: 0.84 ± 0.05). e) GO analysis (biological process) indicates that genes ($n = 186$) rescued by *daw*$^{c458/+}$ are highly enriched in innate immune pathways. f) The *Daw* gene locus and a diagram for a small deletion generated on the 3′UTR of Daw transcript. The CRISPR/Cas9 method was used to induce site-specific deletion of 82nt DNA that contained the miR-252 binding sites. g) Flies deficient in both *foxo* and *daw-3′UTR* show strong defect in adult emergence. Eclosed adult flies for indicated genotypes were counted. Genotypes: WT: 5905. *daw-3′UTR*$^{c82/c82}$. *foxo*$^{c431/c431}$. *daw-3′UTR*$^{c82/c82}$; *foxo*$^{c431/c431}$ (for fly quantification: mean ± SD of 10 biological repeats; Student's *t*-test). h) Mutant flies develop strong melanization marks. Melanization counts as in (a). Genotypes: WT: 5905. *daw-3′UTR*$^{c82/c82}$; *foxo*$^{c431/c431}$ (for quantification: mean ± SEM of 3 biological repeats; Student's *t*-test). i) GO analysis (biological processes) reveals an immune hyperactivation in *daw-3′UTR foxo* double mutants. RNA-seq as in (b). Genotypes: WT: 5905. *daw-3′UTR*$^{c82/c82}$; *foxo*$^{c431/c431}$.

nuclei for transcriptome analysis (sNuc-seq) using droplet microfluidics (10× Genomics), which consistently yielded lower sequence reads mapped to mitochondria (Supplementary Fig. 5, b and c). Overall, 81.38% of reads aligned to genomes, among which 65.28% mapped to exons, 8.12% mapped to introns, and 1.36% mapped to intergenic regions. We finally retained 10,209 nuclei for further analysis (5,689 nuclei for WT and 4,520 nuclei for *mir-252*^{c328} *foxo*^{c431} double mutants) (Fig. 5a). On average, each nucleus sample contained between 100 and 2,000 UMIs and between 60 and 900 genes. We obtained similar number and distribution of transcripts and genes per nucleus in WT and double mutants (Supplementary Fig. 5, d and e). Importantly, sNuc-seq showed high concordance when compared with bulk RNA-seq from genotype-matched fly tissues (Supplementary Fig. 5f), validating the performance of sNuc-seq approach.

The 10K filtered cells were clustered using Seurat 3.0 (Stuart et al. 2019) into 17 distinct clusters. We used principal component analysis (PCA) dimension reduction followed by graph-

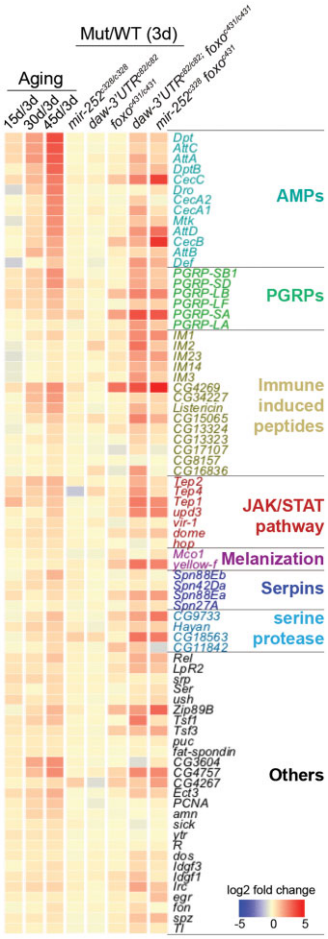

Fig. 4. Loss of *mir-252* and *foxo* accelerates inflammaging. Heat map shows that innate immune genes are upregulated during natural aging, and this pattern of increase is dramatically advanced in 3-day-old mutants of indicated genotypes. RNA-seq was from muscle tissues of female flies. Genotypes: WT: 5905. $atg8a^{c320/c320}$. $mir\text{-}252^{c328/c328}$. $daw\text{-}3'UTR^{c82/c82}$. $foxo^{c431/c431}$. $daw\text{-}3'UTR^{c82/c82}$; $foxo^{c431/c431}$. $mir\text{-}252^{c328}$ $foxo^{c431}$: $mir\text{-}252^{c328}$, $foxo^{c431}$/$mir\text{-}252^{c328}$, $foxo^{c431}$.

based clustering, which was visualized by Uniform Manifold Approximation and Projection (UMAP) (Fig. 5a). Numbers of detected UMIs and genes were comparable among all clusters (Supplementary Fig. 5g). Each cluster contained nuclei from all samples, indicating overall reproducible transcriptional identities between WT and mutants. We performed differential expression analysis to identify marker genes that were significantly enriched in particular clusters. We subsequently defined cell clusters to known cell types based on outspoken signature genes identified in the clusters (Fig. 5b, Supplementary Fig. 6a, and Supplementary Table 5). However, due to the lack of cell-type specific markers, 3 clusters remained unannotated at our UMAP.

We observed major cellular responses between WT and mutants. To determine whether changes in the percentage of cell population were greater than expected by chance, we used a permutation-based analysis as described previously (Farbehi et al. 2019). This analysis revealed a significant increase of hemocytes in double mutants (Fig. 5c), consistent with the observation of $mir\text{-}252^{c328}$ $foxo^{c431}$ flies that exhibited dramatically enhanced melanization. Muscle cells, on the other hand, were decreased, likely reflective of a degenerative process in the mutants (Fig. 5c).

As an activin-like ligand of the TGF-β pathway, the transcription of Daw was mainly found in cells enriched for fat body marker genes (Fig. 5, d and e and Supplementary Fig. 6b), whereas a distinct cell cluster represented transcriptional response of innate immune genes, including the expression of AttB, AttC, DptA, DptB, Dro, and Mtk genes (Fig. 5, d and e and Supplementary Fig. 6b). We therefore named this cluster "activated immune cells." At the single-cell level, expression of Daw and innate immune genes were consistently increased in mutants (Fig. 5e). Taken together, single-cell sequencing analysis reveals that Daw and innate immune genes appear to be expressed in distinct cell types, suggesting a potentially noncell autonomous interaction.

Kenny and Relish are downstream innate immune regulators

To determine the downstream effectors that mediate inflammaging, we asked whether particular immune regulatory genes might be involved. Previous study has implicated a signaling cascade by which Daw activates its downstream effector Smox, a transcriptional repressor, which in turn downregulates the expression of Atg8a gene of the autophagy pathway (Bai et al. 2013). Consistently, in $miR\text{-}252^{c328}$ $foxo^{c431}$ double mutants, Atg8a was transcriptionally downregulated, but the level of decrease was mitigated by daw^{c458} (Fig. 6a).

A recent study has shown that the turnover of Kenny (Key) protein, the *Drosophila* IKKγ homolog of the IκB kinase complex, requires Atg8a protein-mediated selective autophagy (Tusco et al. 2017); we therefore characterized the role of Key. For this study, we constructed a genomic transgene that expressed tagged Key protein under its endogenous pattern (Supplementary Fig. 7a). In $mir\text{-}252^{c328}$ $foxo^{c431}$ double mutants where Atg8a had partial loss, the level of Key protein was elevated as shown by western immunoblot (Fig. 6b). Given this increase at the protein level, we tested whether decrease of Key could rescue the lifespan phenotype. To do this, we generated a deficiency mutant, key^{c369}, by CRISPR/Cas9 mutagenesis (Supplementary Table 4). In the background of key^{c369}, lifespan defect in $mir\text{-}252^{c328}$ $foxo^{c431}$ double mutants were mitigated (Fig. 6c). Moreover, abnormal melanization and induction of innate immune genes were attenuated (Fig. 6, d and e).

Prompted by the report that Relish (Rel) protein, a *Drosophila* NF-κB homolog, is activated by IκB kinase complex-induced proteolytic cleavage (Silverman et al. 2000), we further examined the role of Rel in *mir-252* and *foxo*-regulated hyper-activation of innate immunity. To assess its change at the protein level, we made a genomic transgene with protein tags at both N′ and C′ termini of the Rel protein, such that the cleaved forms could be detected (Fig. 7b). Western immunoblot from muscle tissues identified cleaved forms of the Rel protein being increased in $mir\text{-}252^{c328}$ $foxo^{c431}$ double mutants (Fig. 6f). As was found for Key, the partial loss of Rel using rel^{c975}, a CRISPR/Cas9-derived deficiency (Supplementary Table 4), mitigated the defects in $mir\text{-}252^{c328}$ $foxo^{c431}$ double mutants, including lifespan (Fig. 6g), melanization (Fig. 6h), and the expression of innate immune genes (Fig. 6i). These data together determine that Key and Rel are downstream regulators that contribute to the abnormal induction of innate immune genes in the double mutants.

FoxO, Atg8a, and miR-252 promote longevity by repressing inflammaging

Notably, our recent study has noted that Daw signaling is increased in old flies (Chang et al. 2020). We therefore interrogated how aging affected FoxO pathway factors and whether

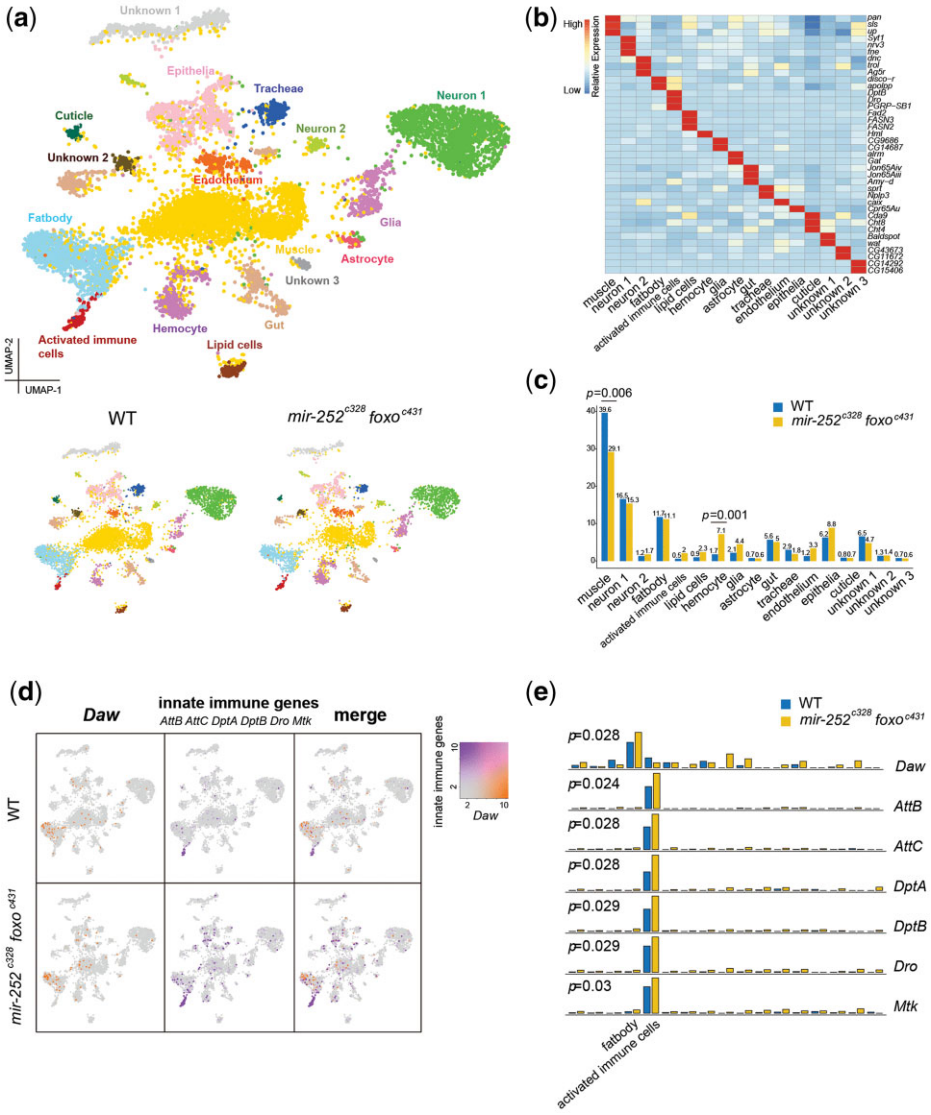

Fig. 5. sNuc-seq reveals cell-specific expression for Daw and innate immune genes. a) Visualization by UMAP plots of clustering of all 10,209 single-nucleus expression profile (top panel), and of WT and double mutants (bottom panel). Each dot represents a single nucleus that is color coded by cell type. Single-nucleus RNA-seq was from muscle tissues of 3-day-old female flies. Genotypes: WT: 5905. *mir-252*^{c328} *foxo*^{c431}: *mir-252*^{c328}, *foxo*^{c431}/*mir-252*^{c328}, *foxo*^{c431}. b) Heatmap showing expression of cluster-specific genes in cell groups defined in (a). c) Cell population percentages between WT and *mir-252*^{c328} *foxo*^{c431} double mutants determined to be significantly modulated according to differential proportion analysis ($P < 0.01$). d) Expression of Daw and innate immune genes (AttB, AttC, DptA, DptB, Dro, and Mtk) genes as visualized on UMAP plots. e) Relative expression of *Daw* and innate immune genes as indicated in distinct clusters between WT and *mir-252*^{c328} *foxo*^{c431} double mutants.

modulation of FoxO and miR-252 in WT flies could repress inflammaging. Analysis of aging transcriptome from muscle tissues showed that FoxO and its upstream regulator Pten (Stambolic et al. 1998; Oldham et al. 2002) and its downstream effectors Thor and Atg8a were decreased in gene expression with age (Fig. 7a). Concomitant with their transcriptional decline, FoxO and Atg8a proteins, as indicated by genomic transgenes of tagged proteins (Supplementary Fig. 8a), were reduced in aged compared to young flies (Fig. 7b). In contrast, the levels of Key and Rel proteins were instead upregulated (Fig. 7b).

Given these results, we tested whether increased expression of FoxO, miR-252, and Atg8a in WT flies could retard inflammaging. Assessment of lifespan indicated that, overexpression of FoxO, miR-252, and Atg8a by genomic transgenes promoted longevity (extension from 12% to 20% of median lifespan) (Fig. 7c). An independent lifespan analysis was performed with similar results (Supplementary Fig. 8b). Coupled with lifespan extension, the age-induced innate immune genes were substantially attenuated upon overexpression of FoxO, miR-252, or Atg8a under their endogenous patterns (Fig. 7d). These results combined with above evidence demonstrate that inflammaging might be induced by a parallel reduction of FoxO activity and that pro-life benefits of FoxO pathway factors and miR-252 might be at least in part attributed to their effect in repressing Daw-mediated inflammaging.

Discussion

The expression of pro-inflammatory genes in older individuals becomes spontaneously upregulated, conferring negative impacts on adult lifespan. Thus, a question in the biology of

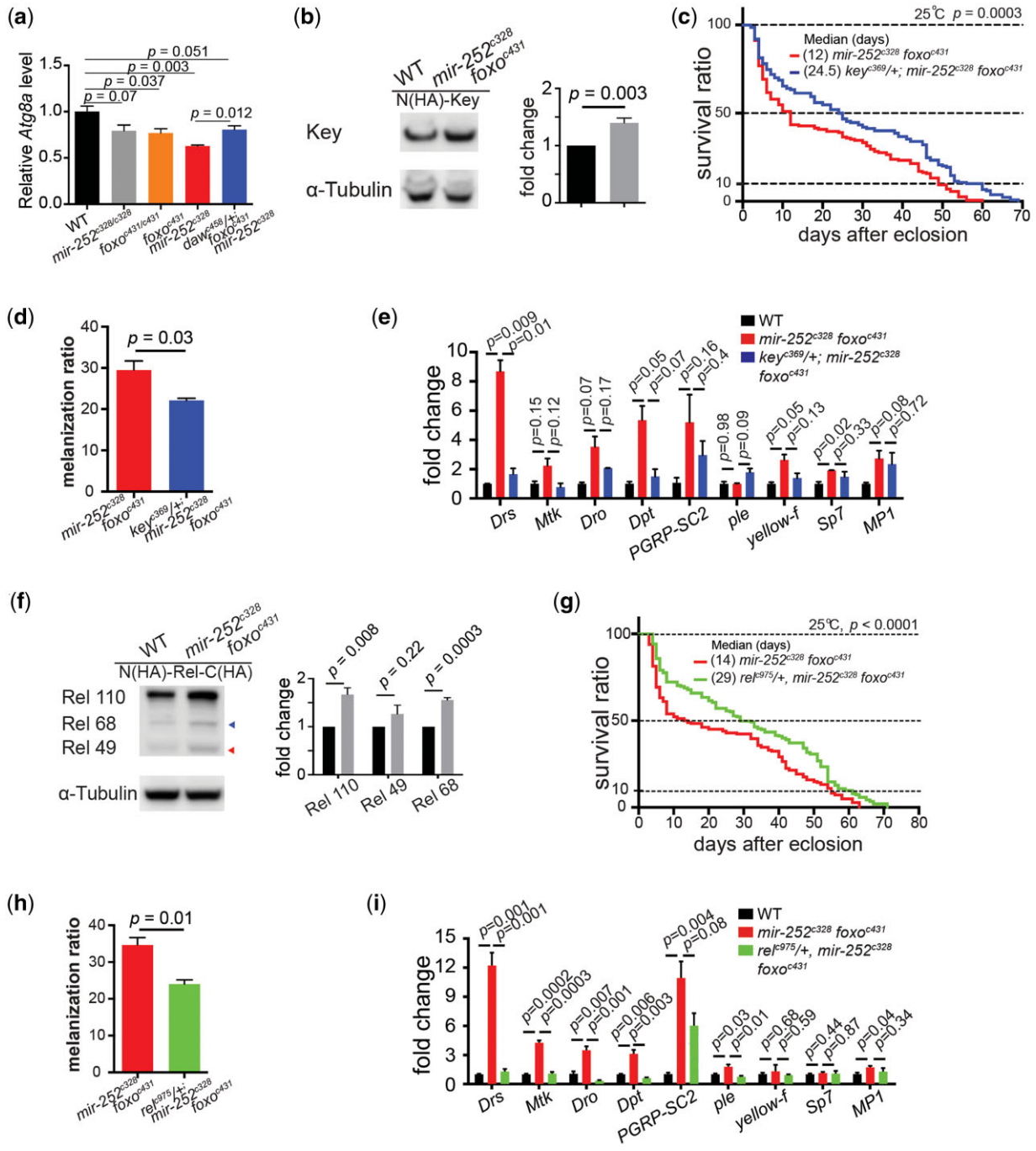

Fig. 6. Kenny and Relish are downstream innate immune regulators. a) Atg8a is downregulated in *miR-252 foxo* double mutants, but this decrease is partially rescued by *daw* deficiency. Normalized read counts from RNA-seq datasets were used. RNA-seq was from muscle tissues of 3-day-old female flies. Genotypes: WT: 5905. *mir-252*$^{c328/c328}$. *foxo*$^{c431/c431}$. *mir-252*^{c328} *foxo*^{c431}: *mir-252*^{c328}, *foxo*^{c431}/*mir-252*^{c328}, *foxo*^{c431}. *daw*^{c458}/+; *mir-252*^{c328} *foxo*^{c431}: *daw*^{c458}/+; *mir-252*^{c328}, *foxo*^{c431}/*mir-252*^{c328}, *foxo*^{c431} (for quantification: mean ± SEM of 3 biological repeats; Student's *t*-test). b) The steady-state level of Key protein is significantly increased in *miR-252 foxo* double mutants. Western immunoblot was from muscle tissues of 3-day-old female flies. Genotypes: WT: pBID-genomic-N(HA)-Key/+. *mir-252*^{c328} *foxo*^{c431}: pBID-genomic-N(HA)-Key/+; *mir-252*^{c328}, *foxo*^{c431}/*mir-252*^{c328}, *foxo*^{c431} (for quantification: mean ± SEM of 3 biological repeats; Student's *t*-test). Reducing Key partially rescues defects in *mir-252 foxo* double mutants, including lifespan c), melanization d), and innate immune induction e). qRT-PCR analysis was from muscle tissues of 3-day-old female flies. Genotypes: *mir-252*^{c328} *foxo*^{c431}: *mir-252*^{c328}, *foxo*^{c431}/*mir-252*^{c328}, *foxo*^{c431} and *key*^{c369}/+; *mir-252*^{c328} *foxo*^{c431}: *key*^{c369}/+; *mir-252*^{c328}, *foxo*^{c431}/*mir-252*^{c328}, *foxo*^{c431} (for lifespan assay: 25°C; $n \geq 200$ female flies per genotype for curve; log-rank test (for quantification of melanization marks: mean ± SD of 3 biological repeats with more than 50 flies for each replicate. For quantification of qRT-PCR result: mean ± SE of 3 biological repeats; Student's *t*-test). f) The Rel protein and its cleaved forms (indicated by arrowhead) are increased in *miR-252 foxo* double mutants. Western immunoblot and quantification as in (b). Genotypes: WT: pBID-genomic-N(HA)-Rel-C(HA)/+. *mir-252*^{c328} *foxo*^{c431}: pBID-genomic-N(HA)-Rel-C(HA)/+; *mir-252*^{c328}, *foxo*^{c431}/*mir-252*^{c328}, *foxo*^{c431}. *rel* deficiency partially rescues defects in *mir-252 foxo* double mutants, including lifespan g), melanization h), and innate immune induction i). Lifespan assay as in (c), melanization count as in (d), and qRT-PCR as in (e). Genotypes: *mir-252*^{c328} *foxo*^{c431}: *mir-252*^{c328}, *foxo*^{c431}/*mir-252*^{c328}, *foxo*^{c431} and *rel*^{c975}/+; *mir-252*^{c328} *foxo*^{c431}: *rel*^{c975}/+; *mir-252*^{c328}, *foxo*^{c431}/*mir-252*^{c328}, *foxo*^{c431}.

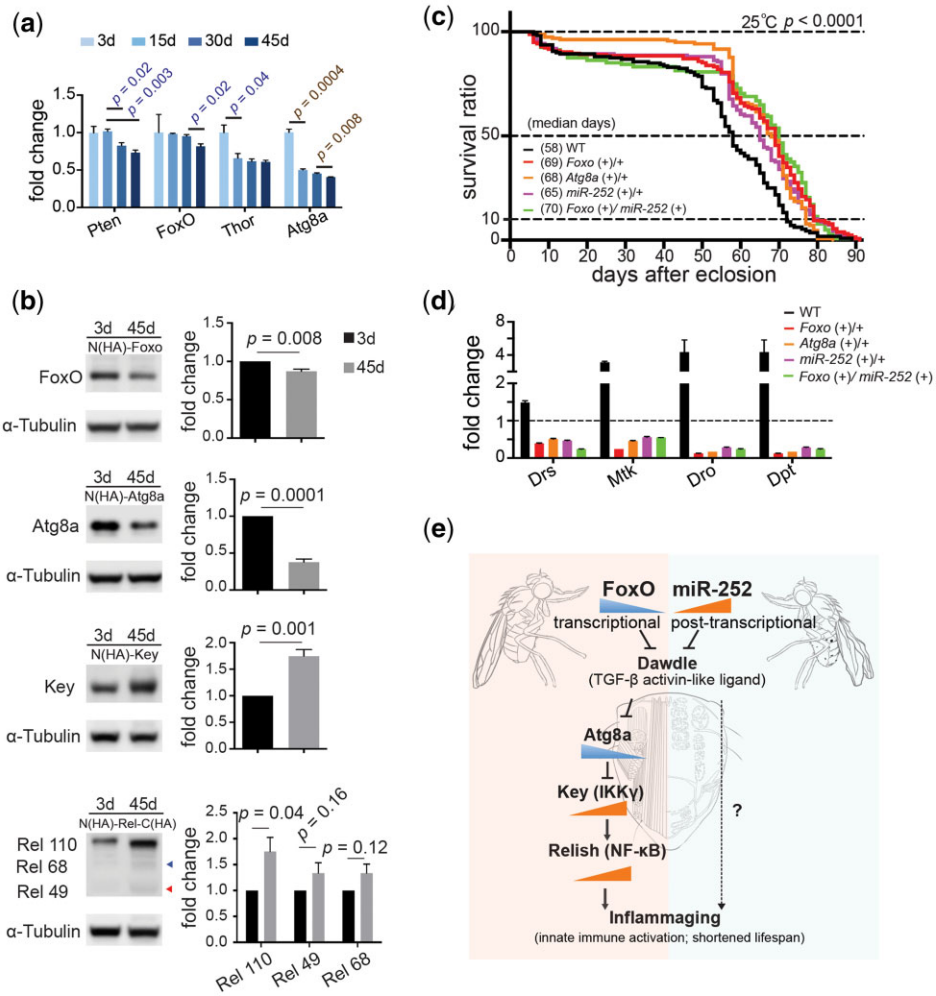

Fig. 7. FOXO signaling pathways promote adult survival by repressing inflammaging. a) FOXO signaling components, including Pten, FoxO, Thor, and Atg8a, show decreased expression with age. Normalized read counts from RNA-seq datasets of indicated age relative to 3 days were used. RNA-seq was from muscle tissues of female flies. Genotypes: WT: 5905 (for quantification: mean ± SEM of 3 biological repeats; Student's *t*-test). b) Western immunoblot shows that while FoxO and Atg8a proteins become reduced with age, Key and Rel proteins are instead upregulated. Western immunoblot was from muscle tissues of 3- and 45-day-old female flies. Genotypes: pBID-genomic-N(HA)-FoxO/+. pBID-genomic-N(HA)-Atg8a/+. pBID-genomic-N(HA)-Key/+ and pBID-genomic-N(HA)-Rel-C(HA)/+ (for quantification: mean ± SEM of 3 biological repeats; Student's *t*-test). c) Genomic transgene of miR-252, Foxo, and Atg8a promotes longevity. Genotypes: WT: 5905. FoxO (+)/+: pBID-genomic-N(HA)-FoxO/+. *Atg8a* (+)/+:pBID-genomic-N(HA)-*Atg8a*/+. miR-252 (+)/+: pBID-genomic-miR-252/+ and Foxo (+)/miR-252 (+): pBID-genomic-N(HA)-Foxo/pBID-genomic-miR-252 (for lifespan assay: 25°C; $n \geq 200$ female flies per genotype for curve; log-rank test). d) Age-associated innate immune genes are downregulated. Genotypes as in (c). qPCR analysis was from muscle tissues of 3- and 45-day-old female flies (for quantification: mean ± SEM of 3 biological repeats; Student's *t*-test). e) Model. FoxO, a conserved transcriptional factor, and miR-252 negatively regulate Daw, at the transcriptional and post-transcriptional level, respectively. Activated Daw causes the reduction of Atg8a-mediated selective autophagy on Key/IKKγ protein, which in turn activates Rel/NF-κB protein and consequentially upregulation of innate immune genes. During natural aging, while miR-252 is increased, FOXO signaling is decreased. As a consequence, Key, Rel proteins, and expression of downstream innate immune genes become increased. Activities of Key and Rel might not be sufficient to mediate all aspects of observed gene profiles, and it is possible, as indicated by the question mark, that additional immune regulators might be involved. Combined, miR-252 and FoxO repress inflammaging through dual inhibition on Daw of TGF-β pathway.

aging is to identify the genes and pathways that refrain inflammaging. Our study in *Drosophila* reveals a dual-inhibitory mechanism by miR-252 and FoxO, to mitigate Daw-induced innate immune genes in aging animals (Fig. 7e). Our genetic evidence demonstrates an intracellular signaling cascade downstream of Daw by decreasing the expression of Atg8a which in turn increases Key and Rel of immune effectors, to promote inflammaging. Transgenic increase of miR-252 and FoxO pathway factors in WT *Drosophila* extends lifespan and mitigates the expression of age-associated induction of innate immune genes.

miRNAs have emerged as critical modulators in post-transcriptional gene regulation. While each miRNA may be predicted to potentially regulate hundreds of target genes (Bartel 2009), it is possible that many miRNAs exert their physiological roles mainly through just a few target mRNAs. As noted, *Drosophila* genome encodes 258 distinct miRNAs (Kozomara and Griffiths-Jones 2014). We were able to detect 110 miRNAs present in adult head and muscle of post-mitotic tissues, corresponding to 1,161 candidate mRNA targets as identified by miRNA targetomes. While some candidate targets modulate the biological processes relevant to post-mitotic and fully differentiated cell fate, it is noteworthy that significant amounts of enriched mRNAs from adult AGO1 RIP-seq are developmental genes, e.g. Egfr and Fng of imaginal disc development, Blimp-1 of respiratory system development, Kni and Mew of neural development,

among others. Our previous report notes that some of age-associated effects of fly miR-34 require adult-onset silencing of Eip74EF gene, an ETS domain transcription factor essentially involved in steroid hormone pathways during development (Liu et al. 2012). If this mode of regulation expands into additional developmental genes and processes as implicated by the present study, one of the roles that miRNAs might play in the adult stage is to tune down developmental genes, thereby promoting adult transition and physiology.

The current study provides the first atlas of miRNA-regulated targets and their temporal dynamics in the adult life cycle, a resource that allows in-depth functional characterization of specific miRNAs and their targets. Based on this knowledge, we further reveal Daw as a direct target of miR-252. It is important to mention that many miRNA null mutants yield no discernible phenotypes (Yamagishi et al. 2015; Sherrard et al. 2017); thus, the question of how significant a role of particular miRNA plays in gene regulation remains open. Our findings suggest that FoxO protein coordinates with miR-252 to achieve the robust silencing on Daw gene, at the transcriptional and post-transcriptional levels, respectively. While *mir-252* single mutant exhibits mild phenotype, *mir-252* and *foxo* double mutants yield much stronger deficits than either single mutant alone. We propose that miR-252 activity, enhanced by its age-modulated expression, defines a safeguard mechanism that controls the induction of inflammation as a result of fluctuations in the activity of FoxO protein. Our study suggests a paradigm by which miRNA pathways coordinate with transcriptional regulatory mechanism to tightly control the output of gene expression.

FOXO signaling has been implicated in a wide range of biological processes. Whereas FoxO protein by itself can directly transactivate a small number of genes encoding AMPs upon microbial infection (Becker et al. 2010), we present evidence that reducing FoxO elevates the activity of key immune factors and spontaneous induction of a much broader category of genes pertaining to chronically activated innate immunity. Consistently, FoxO4-null mice exhibit higher basal levels in mucosal immunity compared to WT littermates (Zhou et al. 2009), which aligns with the report that murine TGF-β pathway promotes cellular senescence and cardiac aging marked with strong pro-inflammatory responses (Lyu et al. 2018). These findings together with our data heighten a conserved mechanism that may underline innate immune homeostasis from *Drosophila* to mammals. Given our genetic evidence in flies, it is tempting to speculate a crosstalk between FOXO and TGF-β in the regulation of inflammaging in mammalian system.

Previous bulk gene expression studies show the induction of innate immune genes during inflammaging. However, direct assessment of cell types that mediates this transcriptional response has not yet been available. In the current study, we provide genetic evidence that Daw, encoding an activin-like ligand, can advance inflammaging if not properly regulated. It is therefore an intriguing question as to how exactly a ligand transduces this highly interconnected event within a tissue microenvironment. We used single-nucleus RNA-seq of fly tissues to identify transcriptomic changes in specific cell types. Our results show that Daw transcript is primarily found in the cells enriched for fat body marker genes, while innate immune genes are expressed in distinct cell clusters. Although we cannot determine whether these cell types are completely different or same cells under distinct states, our data potentially indicates a cell non-autonomous regulation from Daw to the induction of innate immunity. Despite the fact that our sNuc-seq approach detects a lower number of RNA than single-cell RNA-seq, as it excludes transcripts outside the nucleus, it is still sensitive to capture cell-type specific transcriptional response, if dramatic enough, consequential to the activation of Daw. Single-nucleus RNA-seq, on the other hand, holds the technical advantages when applied to tissues that have extraordinary diversity of cell morphology, size, and mitochondria content.

Finally, our recent data in *Drosophila* reveals that the number of FoxO-bound genes reduces dramatically in older animals (Birnbaum et al., 2019). Our current study further determines an age-dependent decline in gene expression of FoxO pathway factors, thus in good congruence with the finding that the activity of FOXO signaling is decreased during normal aging. Consistently, Daw signaling has been shown to increase in old flies (Chang et al. 2020). In a reciprocal experiment, transgenic increase of FoxO pathway factors and miR-252 under their endogenous patterns in WT animals is sufficient to promote longevity and mitigate age-associated induction of innate immune genes. These observations, as well as the insight from previous studies, suggest that the initiation of inflammaging might be at least partially attributed to age-associated decline in the FOXO signaling.

Data availability

The raw data files of sequencing experiments have been deposited in the NCBI Gene Expression Omnibus, as well as normalized count and differential expression results generated from DESeq. For bulk RNA-seq, the accession number is GSE124504. For single cell/nucleus RNA-seq, the accession number is GSE142655.

Supplemental material is available at *GENETICS* online.

Acknowledgment

We thank Prof. Junying Yuan for providing considerable support, advice on the experiments, and critical suggestions on the manuscript.

Funding

This work was supported by grants from the National Natural Science Foundation of China to NL (91849109) and YZ (31671428), National Program on Key Basic Research Project of China to NL and YZ (2016YFA0501900 and 2016YFA0501904), and Shanghai Municipal Science and Technology Major Project to NL and YZ (2019SHZDZX02).

Conflicts of interest

RL is affiliated with Singlera Genomics, a company providing customized next-generation sequencing services. The author has no financial interests to declare. The other authors declare that no competing interests exist.

Literature cited

Adler AS, Sinha S, Kawahara TLA, Zhang JY, Segal E, Chang HY. Motif module map reveals enforcement of aging by continual NF-kappaB activity. Genes Dev. 2007;21(24):3244–3257.

Alic N, Andrews TD, Giannakou ME, Papatheodorou I, Slack C, Hoddinott MP, Cochemé HM, Schuster EF, Thornton JM, Partridge L. Genome-wide dFOXO targets and topology of the

transcriptomic response to stress and insulin signalling. Mol Syst Biol. 2011;7:502.

Anders S, Huber W. Differential expression analysis for sequence count data. Genome Biol. 2010;11(10):R106.

Anders S, Pyl PT, Huber W. HTSeq–a Python framework to work with high-throughput sequencing data. Bioinformatics. 2015;31(2):166–169.

Bai H, Kang P, Hernandez AM, Tatar M. Activin signaling targeted by insulin/dFOXO regulates aging and muscle proteostasis in Drosophila. PLoS Genet. 2013;9(11):e1003941.

Bartel DP. MicroRNAs: target recognition and regulatory functions. Cell. 2009;136(2):215–233.

Becker T, Loch G, Beyer M, Zinke I, Aschenbrenner AC, Carrera P, Inhester T, Schultze JL, Hoch M. FOXO-dependent regulation of innate immune homeostasis. Nature. 2010;463(7279):369–373.

Bidla G, Dushay MS, Theopold U. Crystal cell rupture after injury in Drosophila requires the JNK pathway, small GTPases and the TNF homolog Eiger. J Cell Sci. 2007;120(Pt 7):1209–1215.

Birnbaum A, Wu X, Tatar M, Liu N, Bai H.Age-Dependent Changes in Transcription Factor FOXO Targeting in Female Drosophila. Front Genet. 2019;10:10.3389/fgene.2019.00312.

Brummel T, Abdollah S, Haerry TE, Shimell MJ, Merriam J, Raftery L, Wrana JL, O'Connor MB. The Drosophila activin receptor baboon signals through dSmad2 and controls cell proliferation but not patterning during larval development. Genes Dev. 1999;13(1):98–111.

Cao Y, Chtarbanova S, Petersen AJ, Ganetzky B. Dnr1 mutations cause neurodegeneration in Drosophila by activating the innate immune response in the brain. Proc Natl Acad Sci U S A. 2013;110(19):E1752–1760.

Chang K, Kang P, Liu Y, Huang K, Miao T, Sagona AP, Nezis IP, Bodmer R, Ocorr K, Bai H. TGFB-INHB/activin signaling regulates age-dependent autophagy and cardiac health through inhibition of MTORC2. Autophagy. 2020;16(10):1807–1816.

Chen H, Jacobs E, Schwarzschild MA, McCullough ML, Calle EE, Thun MJ, Ascherio A. Nonsteroidal antiinflammatory drug use and the risk for Parkinson's disease. Ann Neurol. 2005;58(6):963–967.

Chen H, Zheng X, Zheng Y. Age-associated loss of lamin-B leads to systemic inflammation and gut hyperplasia. Cell. 2014;159(4):829–843.

Chi SW, Zang JB, Mele A, Darnell RB. Argonaute HITS-CLIP decodes microRNA-mRNA interaction maps. Nature. 2009;460(7254):479–486.

De Gregorio E, Spellman PT, Tzou P, Rubin GM, Lemaitre B. The Toll and Imd pathways are the major regulators of the immune response in Drosophila. EMBO J. 2002;21(11):2568–2579.

Demontis F, Patel VK, Swindell WR, Perrimon N. Intertissue control of the nucleolus via a myokine-dependent longevity pathway. Cell Rep. 2014;7(5):1481–1494.

Demontis F, Perrimon N. FOXO/4E-BP signaling in Drosophila muscles regulates organism-wide proteostasis during aging. Cell. 2010;143(5):813–825.

Dobin A, Davis CA, Schlesinger F, Drenkow J, Zaleski C, Jha S, Batut P, Chaisson M, Gingeras TR. STAR: ultrafast universal RNA-seq aligner. Bioinformatics. 2013;29(1):15–21.

Easow G, Teleman AA, Cohen SM. Isolation of microRNA targets by miRNP immunopurification. RNA. 2007;13(8):1198–1204.

Farbehi N, Patrick R, Dorison A, Xaymardan M, Janbandhu V, Wystub-Lis K, Ho JW, Nordon RE, Harvey RP. Single-cell expression profiling reveals dynamic flux of cardiac stromal, vascular and immune cells in health and injury. Elife. 2019;8:e43882.

Franceschi C, Bonafè M, Valensin S, Olivieri F, De Luca M, Ottaviani E, De Benedictis G. Inflamm-aging. An evolutionary perspective on immunosenescence. Ann N Y Acad Sci. 2000;908:244–254.

Friedländer MR, Chen W, Adamidi C, Maaskola J, Einspanier R, Knespel S, Rajewsky N. Discovering microRNAs from deep sequencing data using miRDeep. Nat Biotechnol. 2008;26(4):407–415.

Garbuzov A, Tatar M. Hormonal regulation of Drosophila microRNA let-7 and miR-125 that target innate immunity. Fly (Austin). 2010;4(4):306–311.

Guo L, Karpac J, Tran SL, Jasper H. PGRP-SC2 promotes gut immune homeostasis to limit commensal dysbiosis and extend lifespan. Cell. 2014;156(1–2):109–122.

Hedengren M, BengtÅsling Dushay MS, Ando I, Ekengren S, Wihlborg M, Hultmark D. Relish, a Central Factor in the Control of Humoral but Not Cellular Immunity in Drosophila. Molecular Cell. 1999;4:827–837. 10.1016/S1097-2765(00)80392-5.

Huang da W, Sherman BT, Lempicki RA. Bioinformatics enrichment tools: paths toward the comprehensive functional analysis of large gene lists. Nucleic Acids Res. 2009;37(1):1–13.

Hwangbo DS, Gershman B, Gersham B, Tu M-P, Palmer M, Tatar M. Drosophila dFOXO controls lifespan and regulates insulin signalling in brain and fat body. Nature. 2004;429(6991):562–566.

Kheradpour P, Stark A, Roy S, Kellis M. Reliable prediction of regulator targets using 12 Drosophila genomes. Genome Res. 2007;17(12):1919–1931.

Kiselev VY, Andrews TS, Hemberg M. Challenges in unsupervised clustering of single-cell RNA-seq data. Nat Rev Genet. 2019;20(5):273–282.

Kops GJPL, Dansen TB, Polderman PE, Saarloos I, Wirtz KWA, Coffer PJ, Huang T-T, Bos JL, Medema RH, Burgering BMT. Forkhead transcription factor FOXO3a protects quiescent cells from oxidative stress. Nature. 2002;419(6904):316–321.

Kozomara A, Griffiths-Jones S. miRBase: annotating high confidence microRNAs using deep sequencing data. Nucleic Acids Res. 2014;42(Database issue):D68–73.

Lee RC, Feinbaum RL, Ambros V. The C. elegans heterochronic gene lin-4 encodes small RNAs with antisense complementarity to lin-14. Cell. 1993;75(5):843–854.

Lemaitre B, Kromer-Metzger E, Michaut L, Nicolas E, Meister M, Georgel P, Reichhart JM, Hoffmann JA. A recessive mutation, immune deficiency (IMD), defines two distinct control pathways in the Drosophila host defense. Proc Natl Acad Sci U S A. 1995;92(21):9465–9469.

Lemaitre B, Nicolas E, Michaut L, Reichhart JM, Hoffmann JA. The dorsoventral regulatory gene cassette spatzle/Toll/cactus controls the potent antifungal response in Drosophila adults. Cell. 1996;86(6):973–983.

Liu N, Landreh M, Cao K, Abe M, Hendriks G-J, Kennerdell JR, Zhu Y, Wang L-S, Bonini NM. The microRNA miR-34 modulates ageing and neurodegeneration in Drosophila. Nature. 2012;482(7386):519–523.

Lun ATL, Riesenfeld S, Andrews T, Dao TP, Gomes T, participants in the 1st Human Cell Atlas Jamboree, Marioni JC. EmptyDrops: distinguishing cells from empty droplets in droplet-based single-cell RNA sequencing data. Genome Biol. 2019;20(1):63.

Lyu G, Guan Y, Zhang C, Zong L, Sun L, Huang X, Huang L, Zhang L, Tian X-L, Zhou Z, *et al.* TGF-beta signaling alters H4K20me3 status via miR-29 and contributes to cellular senescence and cardiac aging. Nat Commun. 2018;9(1):2560.

Malmevik J, Petri R, Klussendorf T, Knauff P, Åkerblom M, Johansson J, Soneji S, Jakobsson J. Identification of the miRNA targetome in hippocampal neurons using RIP-seq. Sci Rep. 2015;5:12609.

Maragkakis M, Vergoulis T, Alexiou P, Reczko M, Plomaritou K, Gousis M, Kourtis K, Koziris N, Dalamagas T, Hatzigeorgiou AG. DIANA-microT Web server upgrade supports Fly and Worm miRNA target prediction and bibliographic miRNA to disease

association. Nucleic Acids Res. 2011;39(Web Server issue): W145–148.
McCarthy DJ, Campbell KR, Lun AT, Wills QF. Scater: pre-processing, quality control, normalization and visualization of single-cell RNA-seq data in R. Bioinformatics. 2017;33(8):1179–1186.
McGeer PL, Schulzer M, McGeer EG. Arthritis and anti-inflammatory agents as possible protective factors for Alzheimer's disease: a review of 17 epidemiologic studies. Neurology. 1996;47(2):425–432.
Nappi AJ, Vass E. Melanogenesis and the generation of cytotoxic molecules during insect cellular immune reactions. Pigment Cell Res. 1993;6(3):117–126.
Okamura K, Ishizuka A, Siomi H, Siomi MC. Distinct roles for Argonaute proteins in small RNA-directed RNA cleavage pathways. Genes Dev. 2004;18(14):1655–1666.
Oldham S, Stocker H, Laffargue M, Wittwer F, Wymann M, Hafen E. The Drosophila insulin/IGF receptor controls growth and size by modulating PtdInsP(3) levels. Development. 2002;129(17): 4103–4109.
Pletcher SD, Macdonald SJ, Marguerie R, Certa U, Stearns SC, Goldstein DB, Partridge L. Genome-wide transcript profiles in aging and calorically restricted *Drosophila melanogaster*. Curr Biol. 2002;12(9):712–723.
Ren X, Sun J, Housden BE, Hu Y, Roesel C, Lin S, Liu L-P, Yang Z, Mao D, Sun L, *et al.* Optimized gene editing technology for *Drosophila melanogaster* using germ line-specific Cas9. Proc Natl Acad Sci U S A. 2013;110(47):19012–19017.
Robinson JT, Thorvaldsdóttir H, Winckler W, Guttman M, Lander ES, Getz G, Mesirov JP. Integrative genomics viewer. Nat Biotechnol. 2011;29(1):24–26.
Sherrard R, Luehr S, Holzkamp H, McJunkin K, Memar N, Conradt B. miRNAs cooperate in apoptosis regulation during *C. elegans* development. Genes Dev. 2017;31(2):209–222.
Silverman N, Zhou R, Stöven S, Pandey N, Hultmark D, Maniatis T. A Drosophila IkappaB kinase complex required for Relish cleavage and antibacterial immunity. Genes Dev. 2000;14(19):2461–2471.
Stambolic V, Suzuki A, de la Pompa JL, Brothers GM, Mirtsos C, Sasaki T, Ruland J, Penninger JM, Siderovski DP, Mak TW. Negative regulation of PKB/Akt-dependent cell survival by the tumor suppressor PTEN. Cell. 1998;95(1):29–39.
Stuart T, Butler A, Hoffman P, Hafemeister C, Papalexi E, Mauck WM, Hao Y, Stoeckius M, Smibert P, Satija R. Comprehensive integration of single-cell data. Cell. 2019;177(7):1888–1902.e1821.
Tusco R, Jacomin A-C, Jain A, Penman BS, Larsen KB, Johansen T, Nezis IP. Kenny mediates selective autophagic degradation of the IKK complex to control innate immune responses. Nat Commun. 2017;8(1):1264.
Vlad SC, Miller DR, Kowall NW, Felson DT. Protective effects of NSAIDs on the development of Alzheimer disease. Neurology. 2008;70(19):1672–1677.
Wang H, Ma Z, Niu K, Xiao Y, Wu X, Pan C, Zhao Y, Wang K, Zhang Y, Liu N. Antagonistic roles of Nibbler and Hen1 in modulating piRNA 3' ends in Drosophila. Development. 2016;143(3):530–539.
Wang JW, Beck ES, McCabe BD. A modular toolset for recombination transgenesis and neurogenetic analysis of Drosophila. PLoS One. 2012;7(7):e42102.
Xu M, Tchkonia T, Ding H, Ogrodnik M, Lubbers ER, Pirtskhalava T, White TA, Johnson KO, Stout MB, Mezera V, *et al.* JAK inhibition alleviates the cellular senescence-associated secretory phenotype and frailty in old age. Proc Natl Acad Sci U S A. 2015;112(46):E6301–6310.
Yamagishi M, Katano H, Hishima T, Shimoyama T, Ota Y, Nakano K, Ishida T, Okada S, Watanabe T. Coordinated loss of microRNA group causes defenseless signaling in malignant lymphoma. Sci Rep. 2015;5:17868.
Yamamoto R, Tatar M. Insulin receptor substrate chico acts with the transcription factor FOXO to extend Drosophila lifespan. Aging Cell. 2011;10(4):729–732.
Zhang G, Li J, Purkayastha S, Tang Y, Zhang H, Yin Y, Li B, Liu G, Cai D. Hypothalamic programming of systemic ageing involving IKK-beta, NF-kappaB and GnRH. Nature. 2013;497(7448):211–216.
Zheng W, Rus F, Hernandez A, Kang P, Goldman W, Silverman N, Tatar M. Dehydration triggers ecdysone-mediated recognition-protein priming and elevated anti-bacterial immune responses in Drosophila Malpighian tubule renal cells. BMC Biol. 2018;16(1):60.
Zhou W, Cao Q, Peng Y, Zhang Q-J, Castrillon DH, DePinho RA, Liu Z-P. FoxO4 inhibits NF-kappaB and protects mice against colonic injury and inflammation. Gastroenterology. 2009;137(4): 1403–1414.

Communicating editor: M. Kuroda